AN ANALYSIS OF ROCKET AND EARTH SATELLITE MEASUREMENTS OF MICROMETEORIC INFLUX

By

CURTIS W. McCRACKEN

Bachelor of Science

Panhandle Agricultural and Mechanical College

Goodwell, Oklahoma

1956

Submitted to the faculty of the Graduate School of
the Oklahoma State University
in partial fulfillment of the requirements
for the degree of
MASTER OF SCIENCE
August, 1959

AN ANALYSIS OF ROCKET AND EARTH SATELLITE

MEASUREMENTS OF MICROMETEORIC INFLUX

Thesis Approved:

Leon W. Schroeder
Thesis Adviser

H. E. Harrington

Dean of the Graduate School

Dedicated

to

W. MERLE ALEXANDER

PREFACE

The recent advent of the Earth satellite and interplanetary probes as exploratory tools in the field of astrophysics has created new and interesting possibilities for astrophysical experiments. One such experiment is the detection of the impacts of micrometeors onto rocket or satellite skins before the micrometeors have interacted with the atmosphere of Earth. In fact, the micrometeor experiment was one of the first experiments to be sent into space, as both Sputnik I and Explorer I (the first of the Earth satellites sent aloft by the Soviet Union and the United States, respectively) had micrometeor detection systems aboard.

Considerable interest has evolved, during the past several years, about the question of the mass distribution of meteoric material. Observations of visual, telescopic, and radar meteors have shown no appreciable deviation from a constant mass per unit visual magnitude relationship, even though considerations of meteoric masses smaller than the radar meteors have kept suggesting a deviation from the constant mass per unit visual magnitude relationship. Such a deviation is expected to occur at some point above (i.e., smaller masses) the radar meteor range.

An analysis of recent rocket and Earth satellite measurements indicates that the mass distribution function very probably does undergo a deviation, and that the seemingly anomalous results of several observations of particulate matter can be explained on the basis of the tentatively revised mass distribution function obtained in the analysis.

ACKNOWLEDGEMENT

I wish to express my most sincere appreciation to everyone who has helped in the preparation of material used in this thesis. Dr. Leon W. Schroeder, my major adviser and thesis supervisor, has been most kind and co-operative in supplying advice and guidance throughout the writing. Special thanks go also to Mr. W. Merle Alexander, who suggested the thesis problem, supplied me with the flight data of the rockets flown by OSU on Contract No. AF 19(604)-1908, and so aptly guided me through the earliest stages of the development of the thesis. My association, both as a student and as a research assistant, with Mr. Alexander has been most enjoyable and enlightening. I wish to thank Mr. Maurice Dubin for the permission to use the flight data as a basis for my thesis and for the several very interesting discussions on micrometeors that we have had at various times.

I would like to thank Dr. H. E. Harrington and Mr. Richard F. Buck, along with the Research Foundation, for the opportunity of working at the Research Foundation Electronics Laboratory during the summer recesses. Due respect is paid also to Messrs. G. R. Huggett, Fred Wenninger, Jr., and Bob Preskitt for their various contributions to the operation of the micrometeor experiment.

Last, but not least, I wish to thank the Special Services Department and Physical Sciences Area of the Oklahoma State University Library for their splendid co-operation in obtaining various items of research literature.

TABLE OF CONTENTS

LIST OF TABLES

LIST OF FIGURES

CHAPTER I

INTRODUCTION AND HISTORICAL SKETCH

The phenomenon of "shooting stars" has been in existence for many hundreds of years, during which time men have gazed upward into the blackness of night to see the tiny streaks of light. The "shooting stars" probably caused little effect, other than that of producing awe and superstition among the people on Earth, except in the relatively infrequent cases when fragments of shooting stars crashed onto Earth. A few such catastrophic events have even been accompanied by considerable destruction and loss of human life.

The association of shooting stars with atmospheric effects on small particles of matter was not realized until near the end of the 18^{th} century. Brandes and Benzenberg of Germany noticed that the shooting stars appeared at an altitude of about 100 kilometers above the surface of the Earth. On the basis of their observations of the height of appearance of the shooting stars, Brandes and Benzenberg deduced that the shooting stars must be caused by small, material bodies that "burned" upon their passage through the atmosphere of Earth. The shooting stars became known as "meteors" since "meteor" means, literally, "something in the atmosphere".

A considerable amount of work was done during the 19^{th} century towards determining the orbits of the swarms of meteoric particles that appeared as shower meteors. Similar work continued into the 20^{th}

century, and as the orbits for the shower meteors were being worked out, several investigators began studying sporadic meteors. Special meteor expeditions were organized, on which trained observers worked according to planned procedures in gathering data on visual and telescopic meteors.

Two basic problems that plagued investigators for a number of years were that of determining the radiant of a sporadic meteor and that of determining reliable values for the geocentric velocities of the meteors. Reduction of the data of visual meteor observations consistently yielded both hyperbolic and elliptic meteor velocities. The problem of determining reliable meteor velocities was solved only recently through the application of radar techniques to meteor astronomy. Even more recently, radar techniques have been used in the determination of the radiant of a single sporadic meteor. The use of radar techniques in the study of meteors led also to the discovery of daytime meteor showers. Only night-time meteors and meteor showers had been observable before the introduction of the radar techniques into meteor astronomy.

The average number of meteors of a given visual magnitude incident on the whole of Earth during a day has been derived from the data for numerous sets of visual observations. In attempts to explain the meteoric phenomena, several investigators turned to developing theories for the interactions of meteoric material with the atmosphere of Earth. Consideration of the mechanisms of meteor trail formation led to expressions relating the visual magnitude of a meteor to the mass of the meteor. The expressions used to relate visual magnitude to mass at the present time are thought to be correct to within an order of magnitude. The accuracy of the expressions is being improved as more information

about meteoric phenomena is obtained. Estimates of the total amount of meteoric material accreted daily by the Earth have been made on the basis of the sets of visual meteor data and the mass to visual magnitude relationships. All of the mass influx estimates based on visual and radar meteor data have shown a constant mass per unit visual magnitude relationship.

A new area of meteoric research was opened when possible meteoric impacts on a rocket were accidentally discovered in 1949. A special program for studying micrometeor detection with high-altitude rockets was put into operation soon afterwards. An acoustical type of micrometeor detection system had been flown successfully on five rockets by the time the instrumentation of Explorer I (the first artificial Earth satellite to be launched by the United States) was begun. The micrometeor experiment was chosen to accompany the radiation experiment of Van Allen as the two prime experiments aboard Explorer I. Both of the experiments were successful. The lower Van Allen belt of radiation was discovered, and an influx of micrometeors was measured with the acoustical type of micrometeor detection system. The successful operation of the acoustical type of micrometeor detection system on Explorer I served also to demonstrate the feasibility of using the micrometeor experiment as a "piggy-back" experiment on high-altitude vehicles that actually carry other experiments as the prime experiment. Both the theoretical and the practical aspects of the study of the interplanetary matter should make the micrometeor experiment important enough to warrant allocation of entire space vehicles for carrying the micrometeor experiment.

Today, man is probably standing at the very threshold of space, figuratively speaking. In actuality, though, the scientists of today

are faced with the intriguing possibilities of numerous experiments designed to gather information on the composition, space distribution, mass distribution, effects on other astronomical bodies, and motion of the so-called interplanetary matter.

CHAPTER II

STATEMENT OF THE PROBLEM

The primary purposes of this paper may be put into statement form as:

1. an analysis of the data obtained recently through the use of micrometeor detection systems mounted on high-altitude rockets and an Earth satellite, and
2. the presentation of the analysis as an indication of a major deviation from the results expected on the basis of extrapolations of visual and radar meteor data.

Watson (1) extrapolated visual meteor data out to a visual magnitude of +30, which is the radiation pressure limit, in an attempt to predict the influx rates of meteors of higher visual magnitudes and lower masses than the faintest of the visual meteors. Visual and radar meteor data for visual magnitudes of about 0 to about +12, as obtained by various investigators, have shown no appreciable deviation from the constant mass per unit visual magnitude extrapolation introduced by Watson.

Considerations of the particulate matter most effective in producing zodiacal light and solar F corona have indicated space densities of particles several orders of magnitude higher than the space densities predicted on the basis of visual and radar meteor observations. Calculated micrometeor influx rates, based on collections of meteoric material from deep-sea sediment, have appeared several orders of magnitude

higher than the rates based on the constant mass per unit visual magnitude relationship. The discrepancies that are seemingly evidenced by the zodiacal light observations and deep-sea collections suggest a reconsideration of the validity of extrapolating the visual meteor data out to the radiation pressure limit.

The high influx rates suggested by the zodiacal light observations and deep-sea sediment collections, while arousing suspicion as to the validity of the constant mass per unit visual magnitude relationship, were hardly sufficient to justify changing the mass distribution function until more definite indications of an appreciable discrepancy were available. The influx rates for particles of the micrometeor range, as measured on a series of high-altitude rockets and a satellite, exceed the rates predicted by the constant mass per unit visual magnitude relationship by several orders of magnitude. It is hoped that the influx rates measured on these vehicles are significant enough to justify a reconsideration of the mass distribution function for particles smaller than the faintest radar meteors.

A mass distribution function may be determined by plotting the influx rate of meteoric particles into Earth's atmosphere as a function of the mass (or, upon multiplication of the particle mass by an average geocentric velocity, the momentum) of the particles. The measured micrometeor influxes, the calculated zodiacal light values of particle space density, and the experimentally observed radar, telescopic, and visual meteor influxes may be used in the construction of the mass distribution plot. An approximate equation for the new mass distribution function may be determined by a curve fitting procedure. The new mass distribution function appears significantly different from the old mass

distribution function (constant mass per unit visual magnitude) for particles of the zodiacal light and micrometeor range.

The total mass of meteoric material accreted daily by Earth may be determined by integrating the influx rate over the significant range of visual magnitudes. The result of the integration shows a daily accretion of meteoric mass several orders of magnitude higher than the estimates based on the extrapolation of visual meteor data. An additional important consequence of the new mass distribution function is that the major portion of the daily accretion of meteoric mass by Earth is probably contributed by the very small micrometeors.

CHAPTER III

A BRIEF SURVEY OF THE LITERATURE

A search in technical journals for articles that deal specifically with micrometeors yields very few articles. However, there are a sizeable number of articles dealing with visual and telescopic meteors, with most of these articles having been written during the second quarter of the 20th century. Numerous articles on radar meteors and the effects of the influx of visual and radar meteors into Earth's atmosphere have been written since the announcement in 1946 of the discovery by Hey and Stewart (2) of radar reflections from meteor trails.

Since some information usable in a study of micrometeors may be derived from or inferred from the various articles written on visual, telescopic, and radar meteors, a logical procedure seems to be that of reviewing the basic concepts and discoveries associated with meteors in general. A digression into the study of meteors serves well as a setting for the study of micrometeors. The references listed in the survey of the literature consist of the major works on meteors and all available sources of information on micrometeors as they exist and/or are detected high in the atmosphere of Earth.

Opik (3) makes reference to an article written by him in 1922 as probably the first attempt to lay down the basic concepts of a physical theory of meteoric phenomena. (4). Opik's (4) paper included a derivation of general validity between the variable mass and velocity of a

meteor. Also included was the idea that the intensity of observable radiation from a visual meteor is proportional to the rate of ablation of the meteor's mass.

Lindemann and Dobson (5) presented a detailed physical theory of meteors in 1923, but their work has been criticized severely. The work of Lindemann and Dobson was concerned with the formation of air caps on meteors at altitudes in excess of 100 kilometers. The presently accepted view of the problem is that the air cap does not form until the meteor reaches a considerably more dense region of the atmosphere at an altitude of about 70 or 80 kilometers.

Sparrow (6) wrote an article in 1926 in which he tried to point out the shortcomings of the theory advanced by Lindemann and Dobson. Also, Sparrow introduced the idea of collisions between an incoming meteor and individual molecules of air. This idea is one of the more important basic concepts of the physical theory of meteors that are still in popular usage. Lindemann (7) made a fiery reply to Sparrow's article, maintaining that Sparrow had made a vast misinterpretation of the article by Lindemann and Dobson. That Sparrow's ideas have out-lived those of Lindemann and Dobson is evident upon making a quick survey of some of the articles written since 1927 on meteors and meteoric phenomena.

Maris (8) made a significant contribution to the physical theory of meteors when he advanced the idea that the collision of a hypervelocity meteor with a practically stationary molecule of air could result in a miniature explosion on the surface of the meteor. The explosion could remove many atoms of the meteoric material from the surface of the meteor, and a sufficient number of such collisions would result in a complete vaporization of the meteoric mass. Visible radiation is produced,

for Maris' model of a meteor, principally by the secondary collisions of the evaporated meteor atoms with the surrounding air.

Opik (3) refers to a study made by himself which is, he says, "an analysis of allegedly all relevant factors instrumental in the process of ablation and atomization of the meteor substance". (9).

Herlofson (10) used some of Opik's results to get the ratios of the portions of a meteor's kinetic energy going into heat, light, and ionization in the meteor trail. The ratios obtained by Herlofson are repeatedly reported in articles written since the appearance of the Herlofson article, and the basis of the ratios is ascribed to the theory developed by Opik. Opik (3) states emphatically that the ratios obtained by Herlofson are based on a misinterpretation by Herlofson of Opik's theory, and that the ratios should not be ascribed to Opik's theory.

Grimminger (11) presents a deceleration equation that is useful for calculating the deceleration of a meteor by the atmosphere. The decelation effect is quite important in the study of micrometeors. Because of their small masses, micrometeors are decelerated quite rapidly upon entering the atmosphere of Earth. Atmospheric parameters for use in the Grimminger deceleration equation may be obtained from Rocket Panel (12) or from the more recent articles by Horowitz and LaGow (13) for the atmosphere above White Sands Proving Ground, New Mexico(hereafter referred to as WSPG) and Horowitz and LaGow (14) for the atmosphere above Fort Churchill, Manitoba, Canada.

An investigation by van de Hulst (15) of the possible methods of production for zodiacal light and solar F corona led van de Hulst to the conclusion that the space density of particles of 0.1 cm to 0.01 cm in

radius was about 10^4 higher than the space density predicted from the observations of visual meteors. Several investigators have considered some of the theoretical and experimental aspects of the sources of zodiacal light and solar F corona. (16, 17, 18). Probably the most widely accepted idea on the production of zodiacal light and solar F corona is that the particles most effective in producing zodiacal light are particles with masses intermediate to the masses of radar meteors and the masses of the smaller micrometeors.

The first known recording of meteoric impacts on a rocket skin occurred on a V-2 rocket fired 8 December 1949. (19). Subsequently, Whipple (20) developed a theory of micrometeorites in which he worked out the necessary conditions for a meteoric mass to be able to reach the ground without having been completely vaporized. A major point of Whipple's theory is that micrometeors are sufficiently small to reradiate the heat gained in collisions with air molecules before vaporization of the micrometeor begins to occur. Whipple coined the name "micrometeorite" for meteoric particles that are small enough to reach the surface of Earth without having been vaporized in their passage through the atmosphere of Earth. A series of papers by various authors contains some information of interest in the study of micrometeors. (21 to 28).

Dubin (19, 29 to 33) has written several articles and papers on the use of instrumentated high-altitude rockets and satellites in the detection of micrometeors. In addition, Dubin has been instrumental in setting up a program of high-altitude rockets on which micrometeor detection systems were carried high into the upper atmosphere. The installation of the acoustical type of micrometeor detection system on Explorer I

was performed under the direction of Dubin. The results obtained by the acoustical type of micrometeor detection system aboard Explorer I have been presented by Dubin (32, 33). The results reported by Dubin for Explorer I have been presented also in published form by Manring (34).

A number of articles useful in the study of meteors and, to some extent, micrometeors appear in Meteors, a book edited by T. R. Kaiser (35).

Berg and Meredith (36) have reported the results of a micrometeor detection system flown on an Aerobee rocket. The results have been analyzed rather critically by Bauer (37).

The micrometeor influx rates measured by the equipment aboard the Soviet Union's Sputnik I have been reported in an article by Manring (34) and by Nazarova (38).

A recently-published book by Opik (3) serves as a welcome summary of the tremendous amount of work on meteors that Opik has done. Most of the important concepts advanced by Opik in earlier(and quite inaccessible) works are summarized by Opik in his recent book.

CHAPTER IV

THEORY PERTINENT TO THE EXPERIMENT

Some aspects of the theory of meteors may be extended to include micrometeors also. A review of some of the basic concepts of meteor theory will serve as a kind of framework on which the theory of micrometeors may be based. A look at some of the features of the solar system may help us to understand the behavior of the micrometeors--our tiny visitors from space.

Collisions Within the Solar System

The major constituents of the solar system are the Sun, the nine planets and their associated moons, a belt of asteroids or minor planets, and a sizeable flock of comets. All of these constituents, except the comets, are imbedded in a lenticular cloud of cosmic dust, with the Sun situated near the center of the cloud. The cosmic dust may also be referred to as meteoric material or interplanetary matter. The planets orbit quite orderly about the Sun, with all the orbits being direct and of fairly low eccentricity. The asteroids orbit about the Sun in a slightly less orderly manner than do the major planets. A certain degree of orderliness is evidenced by the fact that no asteroids with retrograde orbits have been discovered. The orbits of both the major and minor planets all lie fairly close to the ecliptic plane. In contrast, the orbits of the comets may be retrograde or direct and may have any

degree of inclination. A consideration of the material bodies smaller than the asteroids shows that for decreasing particle size, the randomness of the orientation of the orbits of the particles increases.

Of interest to the inhabitants of Earth are the collisions of Earth with the smaller bodies of the solar system as Earth proceeds along in its orbit about the Sun. Most of the collisions of meteoric material with Earth are not noticeable in everyday life. Occasionally, fragments of meteoric material large enough to crash almost unchecked in speed through the atmosphere do penetrate the atmosphere of Earth. Such fragments usually strike the ground with considerable explosiveness. Fortunately, the frequency of collision between Earth and the large fragments is quite low. The fallen fragments of meteoric material are commonly called meteorites.

Meteors are smaller fragments than the meteorites and are characterized by complete vaporization during their plunge through the atmosphere. Meteors are responsible for the streaks of light visible against a dark night sky. Meteors have a higher frequency of occurrence than do the meteorites, and faint meteors occur more frequently than bright meteors. Occurring even more frequently are the telescopic meteors. The telescopic meteors are too faint to be seen with the unaided eye but may be seen with the aid of telescope or binoculars. Of even smaller mass and higher frequency than the telescopic meteors are the radar meteors. Consideration of particles with masses several orders of magnitude lower than the radar meteors leads to a transition into a different class of meteoric particles--the micrometeors. Micrometeors are small enough to be almost stopped in their flight through the atmosphere before appreciable vaporization of the micrometeor occurs. After being practially

stopped, the micrometeors float slowly down through the atmosphere. Micrometeors that reach the ground are called micrometeorities.

Observations of Meteors

A brief review of the basic methods of detecting the influx of meteoric material into the atmosphere of Earth will serve to emphasize a few of the observable parameters associated with the various methods of observing meteors.

Meteorite falls are, fortunately, quite rare, and the observation of a falling meteorite is quite rare indeed. Most meteorites are found a considerable length of time after they have fallen to Earth. Iron meteorites are more easily identified than are the stony meteorites because the stony meteorites and the terrestrial rocks have about the same external appearance.

The brighter visual meteors (-2 to 0. v.m.) may be detected photographically. The low influx rate of photographic meteors makes the photographic method of detection quite expensive and time consuming. Under the Harvard College photographic meteor program, about one meteor was recorded for every 100 hours of exposure time. The visual magnitude of a photographic meteor is one of the parameters deducible from the photograph of the meteor trail. A knowledge of the field of view for the meteor camera allows a computation of the influx rate of photographic meteors of a given visual magnitude.

Trained observers of visual and telescopic meteors may estimate the apparent visual magnitude of a meteor to within about ± 0.5 unit of visual magnitude. Proper corrections must be applied in order to adjust the apparent visual magnitude to apparent zenithal visual magnitude. The

apparent zenithal visual magnitude and the number of meteors entering the observer's field of view in a given interval of time are usable parameters in an analysis of the visual observations. The mass influx rate for a given visual magnitude meteor may be computed, once a relationship between the mass and visual magnitude of the meteor is established. A more detailed treatment of the mass to visual magnitude relationship is presented in Appendix A.

Meteors that are too faint to appear as visual or telescopic meteors may produce trails of ionization of sufficiently high electron densities to reflect radar signals. Electron line density is an important parameter in the study of meteors and the phenomenon of reflection of radar signals from meteor trails. Radar equipment is not capable of determining the visual magnitude of radar meteors, so a relationship relating electron line density to the meteor mass must be derived before the mass influx of radar meteors can be computed. Alternatively, some investigators express their observational results for radar meteors in terms of electron line density and visual magnitude in order to make comparisons to the visual meteor data more convenient.

Visual magnitude is a convenient and meaningful parameter when used in connection with visual and telescopic meteors. Visual magnitude has considerably less meaning for radar meteors, but with the introduction of proper relationships between electron line density and visual magnitude, the term becomes convenient in discussing the radar data. Visual magnitude probably has little if any meaning for meteors smaller than the radar meteors. Neither does visual magnitude have any significant meaning in discussions of micrometeors. However, if a fairly definite relationship could be established between the masses and visual

magnitudes of visual meteors, then this relationship could be extended to include the mass values characteristic of micrometeors. Visual magnitude would then represent a "shorthand" terminology for specifying the mass of a meteor or a micrometeor.

Unfortunately, there are considerable discrepancies in the literature as to the relation between mass and visual magnitude for visual meteors. The mass to visual magnitude relationship contains a luminous efficiency term, and present day indeterminancies of the luminous efficiency allow the mass of a given visual magnitude meteor to be specified only to within an order of magnitude. Most investigators seem to choose the conservatively lower limit for the mass of a given visual magnitude meteor. The choice of a lower luminous efficiency results in larger values for the mass of a given visual magnitude meteor. One of the major problems of present-day meteor physics is that of determining the luminous efficiencies more accurately.

In view of the statements made in the preceding paragraphs about the inadequacy of visual magnitude as a meaningful parameter to be used in discussions of meteoric phenomena, we should investigate the possibilities of finding a better parameter. Mass is a parameter characteristic of all meteoric particles, irrespective of their size. However, as stated previously, the mass of a given visual magnitude visual meteor cannot be given with an accuracy much less than an order of magnitude until the luminous efficiency has been specified. In contrast, the product of the mass of a micrometeor and an average geocentric velocity provides us with an average geocentric momentum for a given mass of micrometeor. The momentum of a micrometeor is an observable parameter with an acoustical type of micrometeor detection system.

Visual magnitude may be used as a very convenient "shorthand" type of notation if a fixed relationship between mass and visual magnitude is adopted. Dubin and the people associated with micrometeor studies at Oklahoma State University (hereafter referred to as OSU) have adopted a mass to visual magnitude relationship by which a visual magnitude of +25 corresponds to a micrometeor with a mass of 1.25×10^{-10} gm and an average geocentric velocity of 40 kilometers per second. The corresponding momentum would be 5×10^{-4} gm cm sec^{-1}. The relationship has been extrapolated in one direction out to the radiation pressure limit and in the other direction to a visual magnitude of less than 0. (See Table I). By this extrapolated relationship, a meteor of 0 visual magnitude has a mass of 1.25 gm--a mass that is less than an order of magnitude greater than the mass of a 0 visual magnitude meteor as given by most investigators. Several investigators have stated explicitly that the mass of a given visual magnitude meteor may be up to an order of magnitude larger than the mass specified by the investigator. Also, Whipple (39) has suggested using the mass of a 0 visual magnitude meteor as 1.25 gm.

Henceforth, in this paper, visual magnitude is used as a "shorthand" terminology according to the following rules and in conjunction with the information listed in Table I.

1. Visual and telescopic meteors are identified by their visual magnitudes (corrected to apparent zenithal visual magnitude by the original investigator, of course).
2. Radar meteors are identified by their visual magnitude, where the visual magnitude has been derived from the electron line density by the original investigator.
3. All particles smaller than the faintest radar meteors

TABLE I

MASS TO VISUAL MAGNITUDE RELATIONSHIP ADOPTED AT OSU

Visual Magnitude (OSU)	Mass of Particle (gm)	Radius of Particle	Momentum of Particle* $\left(\frac{gm\ cm}{sec}\right)$
-10	12500	9.40 cm	5.0×10^{10}
- 7.5	1250	4.36 cm	5.0×10^{9}
- 5	125	2.03 cm	5.0×10^{8}
- 2.5	12.5	0.940 cm	5.0×10^{7}
0	1.25	0.436 cm	5.0×10^{6}
1	0.50	0.322 cm	2.0×10^{6}
2	0.20	0.237 cm	8.0×10^{5}
2.5	0.125	0.203 cm	5.0×10^{5}
3	0.08	0.175 cm	3.2×10^{5}
4	0.031	0.127 cm	1.24×10^{5}
5	1.25×10^{-2}	0.940 mm	5.0×10^{4}
6	5.0×10^{-3}	0.694 mm	2.0×10^{4}
7	2.0×10^{-3}	0.511 mm	8.0×10^{3}
7.5	1.25×10^{-3}	0.436 mm	5.0×10^{3}
8	8.0×10^{-4}	0.322 mm	3.2×10^{3}
9	3.1×10^{-4}	0.237 mm	1.24×10^{3}
10	1.25×10^{-4}	0.203 mm	5.0×10^{2}
11	5.0×10^{-5}	0.175 mm	2.0×10^{2}
12	2.0×10^{-5}	0.127 mm	8.0×10^{1}
12.5	1.25×10^{-5}	94.0 μ	5.0×10^{1}
13	8.0×10^{-6}	69.4 μ	3.2×10^{1}
14	3.1×10^{-6}	51.1 μ	1.24×10^{1}
15	1.25×10^{-6}	43.6 μ	5.0×10^{0}
16	5.0×10^{-7}	32.2 μ	2.0×10^{0}
17	2.0×10^{-7}	23.7 μ	8.0×10^{-1}
17.5	1.25×10^{-7}	20.3 μ	5.0×10^{-1}
18	8.0×10^{-8}	17.5 μ	3.2×10^{-1}
19	3.1×10^{-8}	12.7 μ	1.24×10^{-1}
20	1.25×10^{-8}	9.4 μ	5.0×10^{-2}
21	5.0×10^{-9}	6.9 μ	2.0×10^{-2}
22	2.0×10^{-9}	5.1 μ	8.0×10^{-3}
22.5	1.25×10^{-9}	4.4 μ	5.0×10^{-3}
23	8.0×10^{-10}	3.2 μ	3.2×10^{-3}
24	3.1×10^{-10}	2.4 μ	1.24×10^{-3}
25	1.25×10^{-10}	2.0 μ	5.0×10^{-4}
26	5.0×10^{-11}	1.8 μ	2.0×10^{-4}
27	2.0×10^{-11}	1.3 μ	8.0×10^{-5}
27.5	1.25×10^{-11}	0.9 μ	5.0×10^{-5}
28	8.0×10^{-12}	0.7 μ	3.2×10^{-5}
29	3.1×10^{-12}	0.5 μ	1.24×10^{-5}
30	1.25×10^{-12}	0.4 μ	5.0×10^{-6}
31	5.0×10^{-13}	0.3 μ	2.0×10^{-6}

* $V_G = 40$ Km sec^{-1}

may be identified by their visual magnitude as determined from Table I. Alternatively, either the mass or the average momentum of a micrometeor may be used to describe the particle.

The radii of visual meteors, as given in Table I may not have much meaning if one assumes that the "dust-ball" model is correct for the visual meteors.

Detection of Micrometeors

The momentum of a micrometeor is one of the observable parameters with present-day acoustical type micrometeor detection systems. Therefore, assumption of an average geocentric velocity for the micrometeors allows the masses of the micrometeors to be computed.

Micrometeors may be stopped by the atmosphere before appreciable ionization or vaporization commences. Thus, micrometeors evade detection by both visual and radar techniques. Apparently, the only remaining possibility for detecting micrometeors before they interact with the atmosphere is that of establishing a "platform" in space at some altitude (about 100 kilometers or above) such that the "platform" is above the region of maximum deceleration of the micrometeors. The "platform" could conceivably be a space station in the future. However, at the present time, the only "platforms" available for use in carrying micrometeor detection systems are high-altitude rockets, Earth satellites, and space probes. Sections of rockets stay above altitudes of about 100 kilometers for time intervals measurable in seconds, and space probes soon move out of the immediate neighborhood of Earth. While the movement of the space probes out of the immediate neighborhood of Earth is

a quite welcome accomplishment as far as the experiment is concerned, the problems of telemetry do become more complex for the increasing distance.

There are about three major types of micrometeor detection systems now available for mounting on a space platform. One type of detection system is the acoustical type, in which a crystal microphone is placed in contact with a section of rocket or satellite skin. Micrometeors incident on the sensitive metallic surface register as pulses of microphone output voltage. The output signal pulses may be amplified and transmitted to a ground receiving station. The observable parameters with the acoustical type of micrometeor detection system are the influx rate and the momenta of the incident particles. The determination of the influx rate is based on an assumption that an effective area for the sensitive surface can be specified. An indication of the difficulty of specifying an effective area is included as Appendix B. The acoustical type of micrometeor detection system has passed tests for being momentum sensitive to both elastic and inelastic impacts.

One of the two other types of micrometeor detection systems consists of wire grids which may be broken when a sufficiently large micrometeor strikes the grid. This type of system was used along with the acoustical type system on Explorer I. Manring (34) has reported on the results from the wire-grid type of detection system. The system seemingly suffers from both low effective area and low sensitivity.

The third type of micrometeor detection system has been developed at the Naval Research Laboratory. The system consists basically of a photomultiplier tube facing the metalized surface of a block of lucite. Impacts of meteoric particles onto the metalized surface of the lucite

give rise to tiny flashes of light. The flashes of light are detected, and the corresponding signal is current amplified by the photomultiplier tube. Berg and Meredith (36) have published the results of one flight of this type of micrometeor detection system. The zenith altitude of the flight was only 103 kilometers, which was probably too low for a reliable detection of micrometeors before they had interacted with the atmosphere of Earth. A considerable number of pulses were obtained on the flight, but there seems to be some doubt as to whether all of the pulses were caused by impacts of micrometeors.

One of the chief difficulties encountered in the use of high-altitude rockets as the "platform" is the short data sampling time available. Longer sampling times are needed in order to establish the statistical reliability of the micrometeor counts.

Classes of Meteors

Meteors of all magnitudes may be divided into two general classes--shower and sporadic. Shower meteors occur when the Earth intercepts the common orbital path of a swarm of meteoric particles. The conditions necessary for the production of a meteor shower are illustrated in Figure 1. The conditions shown lead to a night-time meteor shower; a

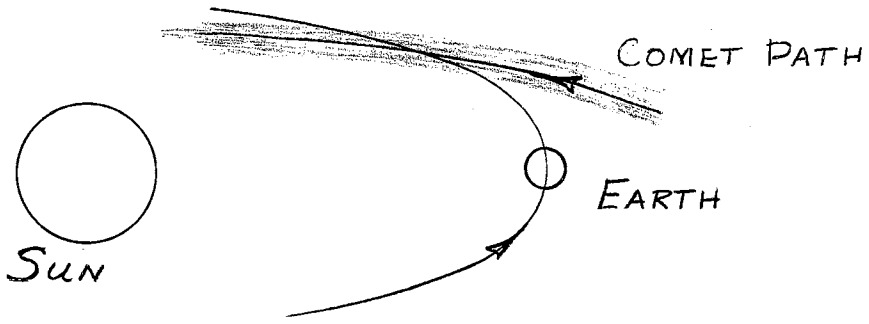

Figure 1. The Production of a Meteor Shower.

daytime meteor shower occurs when the path of the meteoric particles crosses outward across the orbit of Earth.

The duration of the meteor shower is just the time required for the Earth to cross the path of the swarm of particles. Old meteor swarms have the particles distributed along the path of the swarm, while swarms formed by the recent break-up of comets have the particles traveling in bunches.

Meteors that cannot be classed as shower meteors are classed as sporadic meteors. Meteor counts made in the absence of known meteor showers probably consist almost entirely of sporadic meteors. Micrometeors fall into the same two classes as do the meteors. Since the micrometeors do not evidence their plunge into the atmosphere by pronounced visual or radar effects, observations of micrometeor influx cannot be classed as being those of shower or sporadic micrometeors unless some criterion for the classification of the micrometeors can be established.

Studies of shower meteors show that meteor showers are somewhat deficient in fainter meteors. Such a deficiency may be explained quite conclusively by a consideration of the Poynting-Robertson effect on the meteoric particles. Wyatt and Whipple (40) have investigated the action of the Poynting-Robertson effect on meteor orbits. Radiation pressure serves to remove particles of less than about 1 μ diameter from the solar system. The Poynting-Robertson effect is greatest for very small particles that are too large to be removed from the solar system by radiation pressure. Through the action of the Poynting-Robertson effect, the small meteoric particles assume more circular orbits and spiral into the Sun. The smaller particles spiral into the Sun more rapidly than do the larger particles. Several meteor showers have been associated with

comets--the shower meteors are probably just cometary debris. Other meteor showers are thought to be the debris from comets that disappeared long ago. The swarms of meteoric particles have probably made at least several orbits about the Sun, giving the Poynting-Robertson effect time to remove many of the smaller particles from the meteor swarm. Such reasoning implies immediately a shortage of micrometeors in the meteor swarm. If deficiencies in the number of very faint visual meteors are noticeable, then the swarm could certainly be quite deficient in micrometeors, because the micrometeors are several orders of magnitude smaller in size than are the faintest visual meteors.

In view of the supposed deficiency of micrometeors in meteor showers, one must conclude that the most favorable time for measuring micrometeor influxes is probably during non-shower periods. Measurements of micrometeor influxes made during non-shower periods may be assumed to include, for the most part, only sporadic micrometeors. Also, the probability of the rocket being hit by particles large enough to do mechanical damage is considerably lower during the non-shower periods. None of the flights from which the data for this paper come has been during known meteor showers. Hence, the majority of the micrometeors detected are considered to be sporadic micrometeors.

Types of Meteors

Meteors may be classified also according to type by specifying the material of which the meteors are composed. There are stony, iron, and intermediate types of meteors. In general, the shower meteors seem to be predominantly stony in type, while the abundances of sporadic meteors have been given by Allen (41) as 50% iron and 50% stony. As stated

previously, meteor showers are probably deficient in micrometeors. If the micrometeors are predominantly sporadic, then there is a possibility that the numbers of stony and iron micrometeors are at least comparable. The iron micrometeors have densities of approximately 7 gm cm^{-3}, while the stony micrometeors have densities of approximately 1 gm cm^{-3}. An average density must be assumed for use in various computations involving micrometeors. An average density of 3.6 gm cm^{-3} has been used by Whipple (39) and seems to be a suitable value for use in this paper. An average density of 3.6 gm cm^{-3} was used in the derivation of the various quantities listed in Table I.

Velocities of Meteors

The velocity, at 1 astronomical unit from the Sun, of a particle in a parabolic orbit about the Sun is about 42 kilometers per second. One of the primary objectives of the visual meteor observations has been the determination of the geocentric velocities of sporadic meteors. The heliocentric velocity of a meteor can be computed if the geocentric velocity of the meteor, the velocity of the Earth in its orbit, and the radiant of the meteor are known. The diagrams shown in Figure 2 demonstrate the vector addition of the various velocities that yields the heliocentric meteor velocity, u. The geocentric velocity of the meteor is represented by v_g, and the orbital velocity of Earth is represented by v_E.

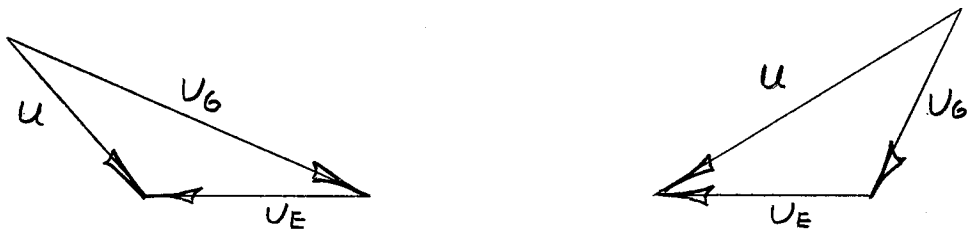

Figure 2. Vector Addition of Meteor Velocities.

The average velocity of Earth along its orbit is 29.8 kilometers per second or approximately 30 kilometers per second. Meteors traveling at the parabolic velocity and meeting the Earth head-on may have a maximum velocity relative to the Earth of about 72 kilometers per second. Similarly, if a parabolic meteor overtakes the Earth from behind, the geocentric velocity of the meteor would be about 11 kilometers per second. The escape velocity of Earth is also about 11 kilometers per second. The range of observable geocentric velocities for meteors, if it is assumed that there are no hyperbolic orbits, would be

$$11 \text{ KM SEC}^{-1} \leq U_G \leq 72 \text{ KM SEC}^{-1}.$$

A velocity of 40 kilometers per second is chosen as the average geocentric velocity of the sporadic meteors and micrometeors. The geocentric velocities for shower meteors depend on the particular meteor shower.

In general, the fast meteors occur during the early morning hours (about 0600 LMT) when the observer is on the forward side of the Earth, and the slow meteors occur in the evening(about 1800 LMT) when the observer is on the trailing side of the Earth. The preceding statements are illustrated in Figure 3.

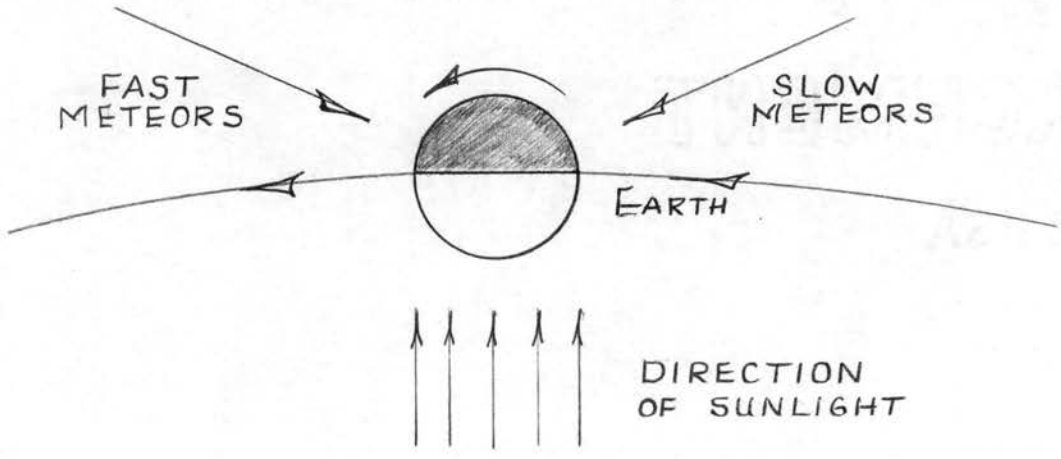

Figure 3. Relative Motion of Earth and Meteors.

Heliocentric velocities in excess of 42 kilometers per second imply hyperbolic orbits for the meteors, while heliocentric velocities of less than 42 kilometers per second imply elliptic orbits for the meteors. Meteors having elliptic orbits are considered to be members of the solar system, while meteors with hyperbolic orbits are considered to be non-members of the solar system. The membership or non-membership of meteoric particles to the solar system forms the basis for quite fundamental and intersting questions in both cosmogony and cosmology.

Observational data taken by trained visual meteor observers have indicated both hyperbolic and elliptic velocities for the meteors. Opik devised a rocking-mirror apparatus in an attempt to determine meteor velocities more accurately, but the apparatus indicated both elliptic and hyperbolic meteor velocities.

The introduction of the use of radar techniques into the study of meteors during and after World War II has represented a major step forward in the study of meteors. McKinley (42) used radar techniques to settle, quite definitely, the question of whether meteors have hyperbolic velocities. The velocities of 10,933 sporadic meteors were measured by McKinley with his radar technique. Not over 0.3% of the meteors seemed to have velocities in excess of 72 kilometers per second. None of the meteors had a velocity in excess of 80 kilometers per second. The few cases of seemingly hyperbolic meteor velocities may be attributed to experimental error. McKinley's work showed that the component of sporadic meteors up to about +8 v.m. having hyperbolic velocities is negligible if existent at all.

The important conclusion that probably no visual or radar meteors have hyperbolic velocities might be extended to include micrometeors

also. However, since some of the visual meteor concepts cannot be extrapolated into the micrometeor range, the author feels that the question concerning the possibility of hyperbolic orbits for micrometeors should be left open until more observational data have been obtained. It is probably far more likely that some of the sporadic micrometeors may be visitors from outside the solar system than for a visual meteor to come from outside the solar system.

The momentum of a micrometeor is a velocity-dependent parameter. The velocity-dependence of the momentum presents a problem just as does the velocity-dependence of the luminosity of visual meteors. A change of unity in visual magnitude corresponds to a change in momentum of 2.5, where the mass has been assumed constant. Since the maximum range for the geocentric velocity with respect to the average value for non-hyperbolic meteors is less than unity, the corresponding maximum range of momentum is less than unity also. The preceding statement means that for a micrometeor of given mass, a change of the geocentric velocity to either the maximum or minimum possible value is not sufficient to change the designation of the particle by unit visual magnitude.

The Mass Distribution of Meteoric Material

The mass distribution of the meteoric material incident on Earth is of considerable interest in the field of astrophysics. Until recently, radar and visual observations have constituted the only means of observing directly the influx of meteoric material. The frequency of occurrence of meteorites is so low as to be of little interest in the study of the mass distribution. Visual meteors occur at an average rate of about 10 per hour for a single observer. A considerable amount of

observational data for visual meteors has been gathered during recent years, with the mass distribution being one of the factors of interest.

More recently, radar techniques have aided in the collection of observational data on meteoric influx and have, in some cases, resolved difficulties common to visual observations. Visual observation or radar observation of micrometeors is not possible because the micrometeors are stopped without producing a significant amount of ionization and without being vaporized.

The masses of incident visual meteors are not experimentally observable quantities. Observed instead are the apparent visual magnitudes of the visual meteors. The apparent visual magnitudes are corrected to zenithal visual magnitudes. The mass distribution function for meteoric particles of the visual meteor range is then obtained by plotting the observed number of meteors as a function of zenithal visual magnitude. Various investigations have shown that for visual meteors, the logarithm of the influx (particles per square meter per second) is a linear function of the visual magnitude. Such a function implies a constant mass influx per unit visual magnitude.

Electron line density replaces visual magnitude as an observable quantity for radar observations. Radar observations have verified the constant mass per unit visual magnitude relationship through the visual and radar ranges of meteors.

Meteoric particles smaller than radar meteors are thought to be at least partially responsible for the zodiacal light. Estimates of the space density of the meteoric particles responsible for zodiacal light exceed the values expected by an extrapolation of the constant mass per unit visual magnitude relationship. The estimated space densities of

particles, as based on zodiacal light measurements, exceed by several orders of magnitude the densities estimated through the use of the extrapolated visual and radar meteor data.

Information about micrometeorites has been obtained through collection of deep-sea sediment, collection of particles that fall with rain, exposure of collecting plates at high altitudes, and micrometeor detection systems flown on high-altitude rockets and satellites. All methods capable of yielding quantitative information on the influx rates have indicated influx rates that were considerably higher than the influx rates predicted by the constant mass per unit visual magnitude relationship.

The preliminary observational results for the described methods of observing micrometeors form the basis for the question: At what visual magnitudes and by how much do the influx rates for meteoric material deviate from the values predicted by the extrapolated data of visual and radar meteors? This question forms one of the major topics of this paper and is left unanswered until later in the paper.

CHAPTER V

COLLECTION OF DATA

The first indication of meteoric impacts on rocket skins appeared on the flight of USAF (United States Air Force) V-2 #31, flown from WSPG on 8 December 1949. Similar indications appeared on another USAF V-2 flown from WSPG on 31 August 1950. Both of these rockets carried an instrumentation that had been developed by Bohn for the purpose of detecting acoustical noise generated in a rocket during the rocket's flight. The instrumentation consisted basically of a crystal microphone placed against the rocket skin, with the output signal of the microphone being amplified and telemetered back to a ground receiving station. The telemetry records of both flights showed pulses which could not be easily attributed to causes within the rocket. The idea that the impacts were those of meteoric particles was advanced by Dubin (30) in order to explain the seemingly spurious pulses.

The data obtained from the two previously mentioned V-2 flights may be, at most, classed as indicative data--data indicative of the fact that something (possibly meteoric particles) was striking the rocket skin and causing the pulses to appear on the telemetry film. The importance of the flights lay in the suggestion of the possibility of sending up acoustical type micrometeor detection apparatus in high-altitude rockets and on Earth satellites. The idea of detecting micrometeor impacts on a rocket skin was strengthened further by the flight of USAF Aerobee #58,

flown on 14 September 1955, with the rocket carrying acoustical type micrometeor detection equipment. The rocket reached zenith at only 100 kilometers, too low for a reliable detection of micrometeors. Pulses that were probably caused by meteoric impacts were found on the telemetry record. The data from this flight must also be classed as indicative data.

USAF Aerobee #77 was instrumentated and calibrated for the detection of micrometeors by the Oklahoma State University Research Foundation Electronics Laboratory. Aerobee #77 was flown from Holloman Air Development Center, New Mexico (hereafter referred to as HADC) on 9 April 1957. This flight carried, in addition to the acoustical type of micrometeor detection system, a highly polished metal plate devised by Bohn. The plate was to be examined, upon recovery, by a photochemical means in order to reveal micrometeor craters in the metal plate. (43). A malfunction of the rocket prevented the rocket from attaining a sufficiently high zenith altitude (zenith was at 26.6 kilometers) for micrometeor counting. The flight was by no means a complete failure, because Yagoda (44) found evidence of meteoric cratering on the recovered metal parts of the rocket. The telemetry record again showed pulses which were probably caused by meteoric impacts. The data from Aerobee #77 must be classed as indicative data.

USAF Aerobees #80 and #81 were the next vehicles to be instrumentated and calibrated at OSU for the purpose of detecting micrometeors. These rockets were flown from HADC on 16 July 1957 and 18 July 1957, respectively. The flight of Aerobee #80 was considered as successful, with the rocket reaching zenith at 121 kilometers. Aerobee #80 had two microphones in contact with the skin of the instrument section of the

rocket and two microphones in contact with a special circular diaphragm that could be exposed by ejection of the nose tip of the rocket after the rocket had made its upward passage through the denser portion of the atmosphere of Earth. The data obtained from the skin-mounted microphones on Aerobee #80 serve as the first reliable micrometeor data of a quantitative nature. The data from the skin of Aerobee #80 are regarded as quantitatively useful for the composite analysis of Chapter IX. The data from the diaphragm-mounted microphones give influx rates that are much higher than the influx rates obtained on any subsequent flights. A completely plausible reason for the high diaphragm counts has not yet been discovered. The diaphragm data may be included in the composite analysis if one remembers that the influx rates determined by the diaphragm are not representative of the influx rates obtained on other flights.

The next set of usable data from vehicles instrumentated and calibrated at OSU was obtained from the flight of USAF Aerobee #88, flown from HADC on 16 October 1957. Aerobee #88 had both skin- and diaphragm-mounted micrometeor detection systems, and data were obtained from both systems. The data from the flight of Aerobee #88 constitute two more sets of quantitatively useful micrometeor influx data.

The first U. S. satellite, Explorer I (or α1958) was launched from Cape Canaveral, Florida, on 31 January 1958. Two types of micrometeor detection systems were carried by Explorer I. One of the systems was of the resistance-wire-grid type, described by Manring (34). This system registered, after ascent, one possible meteoric impact in a period of 60 days. The other micrometeor detection system carried by Explorer I was installed and calibrated under the direction of Alexander of OSU.

Micrometeoric influx data from the acoustical type system was obtained as Explorer I made successive passes over suitably placed ground receiving stations. The micrometeor data obtained from Explorer I has been presented by Dubin (32, 33) and is considered as being quantitatively useful micrometeor influx data.

USAF Cajun AA6.202 was fired from HADC on 1 May 1958, with micrometeor detection equipment constituting the prime experiment aboard. The flight was successful, with data being received by telemetry throughout the flight. Some trouble was experienced with pulses initiated by the thermal expansion of the rocket skin, but the thermally initiated pulses ceased early enough in the usable part of the trajectory that data from most of the usable trajectory were obtained. This flight pointed out the necessity of modifying subsequent Cajun rockets in order to remove the effects of thermally generated pulses. The thermal pulse effect was eliminated from the usable trajectories of subsequent Cajuns by insulating both ends of the rocket skin from the air frame with Teflon bushings. Also, Teflon tape was placed over the contact surfaces of the microphones in order that the expanding rocket skin could slide over the microphones without creating thermal pulses.

USAF Cajuns AA6.204 and AA6.203 were flown from Fort Churchill, Canada, on 14 October 1958 and 15 October 1958, respectively. Cajun AA6.203 reached zenith at 150 kilometers, and Cajun AA6.204 reached zenith at 136 kilometers. USAF Spaerobee AA10.01 was flown from Fort Churchill, Canada, on 22 October 1958, with the rocket attaining an altitude of 176 kilometers. The Spaerobee was fired in hopes of attaining greater altitudes (i.e., longer data sampling times) than those obtained on previous flights. The Sparrow motor was not permitted to fire

because of range safety, resulting in a zenith altitude somewhat lower than was expected. The data from Cajuns AA6.202, AA6.203, and AA6.204 and Spaerobee AA10.01 may be regarded as quantitatively useful micrometeor influx data for the composite analysis presented in Chapter IX.

Detailed descriptions of the individual systems flown on the various flights have been purposely omitted from the preceding paragraphs. A slightly more detailed description of the micrometeor detection systems seems advisable at this point of the discussion. More detailed descriptions of the individual flights have also been prepared as quarterly reports. (45).

Basically, each of the individual micrometeor detection systems consisted of a crystal microphone, a transistorized band-pass amplifier that was tuned to one of the ultrasonic response peaks (about 100 Kcps) of the microphone, and a means of telemetering the output signal of the amplifier to a ground receiving station. A block diagram of a typical micrometeor detection system is shown in Figure 4. The telemetry signal received by the ground receiving station was displayed on a cathode ray oscilloscope, and the display was recorded photographically. The film showed the amplified and shaped output signal of the crystal microphone. The telemetry film serves as a permanent record of the flight data, allowing the record to be checked and rechecked during the analysis of the data.

Both FM-FM and pulse-time telemetry have been used on the various flights. The specification of the type of telemetry or a detailed discussion of the telemetry system of a particular flight does not seem to be essential to the analysis, so such descriptions will not be included in this paper.

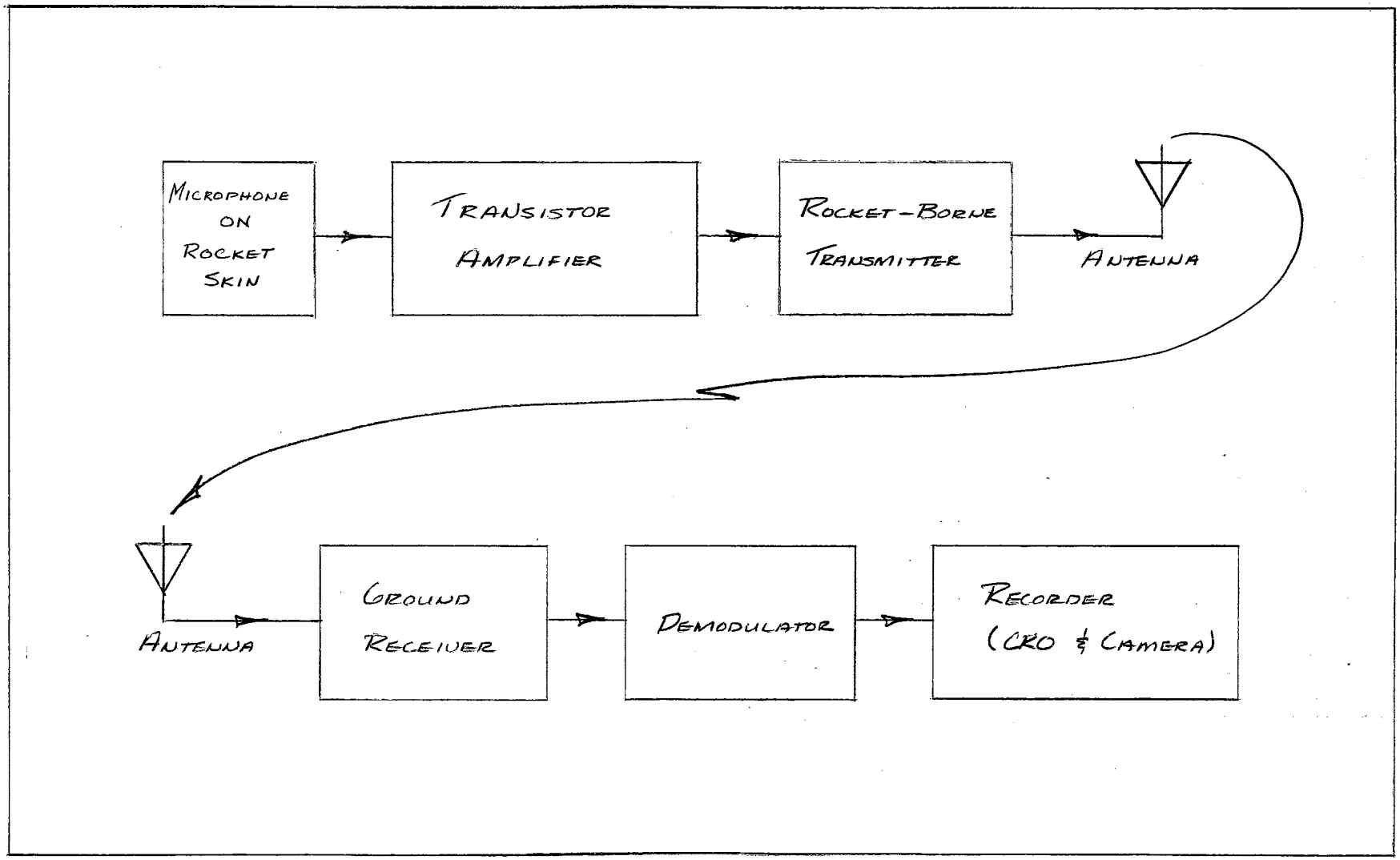

Figure 4. Block Diagram of a Typical Micrometeor Detection System.

The micrometeor detection systems flown on Aerobees #77 and #80 were of the most basic type, consisting of a microphone, amplifier, and a means of telemetering information to ground receiving stations where the data were recorded. The system on each rocket was carefully tested and calibrated before the flight. According to the calibration results, the output voltage of the amplifier was an almost linear function of the momentum of the incident particle over a limited range of momentum. The intelligible output voltage of the amplifier was limited between 0.5 volts and 5.4 volts by the system noise and voltage saturation, respectively. A range of output voltage of 0.5 to 5.0 volts corresponded to a momentum range of 2.5 v.m. Incident particles with momenta larger than the upper limit of the linear region of the response curve caused the amplifier to voltage saturate. When voltage saturated, the amplifier served only as a counter of impacts and not as an indicator of the momentum of an incident particle. Particles with momenta less than the lower limit of the linear region of the response curve did not produce an intelligible pulse at the output of the amplifier. For particles with momenta within the approximately linear region of the response curve, the amplifier served to both count the incident particles and indicate, by means of the magnitude of the output pulse, the momentum of an incident particle. Therefore, the system may be described most simply as being an analog-type system.

More elaborate systems were devised for the subsequent flights. A logarithmic compression circuit was investigated, as the use of such a circuit within the amplifier would have extended the momentum range over which the amplifier output voltage would have been indicative of the momentum of an incident particle. The idea of a compression circuit was

quickly discarded in favor of an ingenious but simple scheme conceived by Alexander. The scheme consisted of placing a voltage tap-off point on the collector of each of the stages of the transistor amplifier. The signal voltage appearing at each of the tap-off points was used in about the same manner as the single output voltage of the original amplifier had been used. The signal voltage appearing at each of the tap-off points proved to be an almost linear function of the momentum of an incident particle for a limited range of momentum. Each tap-off point corresponded to a different range of momentum, and successive stages of the amplifier served adjacent ranges of momentum.

The availability of several voltage tap-off points for a single microphone-amplifier combination led quite naturally to the introduction of digital-type circuits into the micrometeor detection system. Basically, the digital-type circuits consisted of a microphone connected to a high-gain transistorized band-pass amplifier with three to four tap-off points. The signal voltages appearing at the tap-off points were fed into a logic circuit, and the output voltage of the logic circuit was telemetered to the ground. A typical digital-type micrometeor detection system is shown in block diagram form in Figure 5.

Since the various tap-off points represented points of different gain for the amplifier, the system was capable of sorting the pulses caused by impacts of meteoric particles onto the rocket skin into different groups according to the momenta of the incident particles. The analog-type relationship between the magnitude of the output voltage of the amplifier and the momenta of the incident particles was lost upon the introduction of the digital-type system. Most of the digital-type systems had three to four tap-off points, meaning that there were three

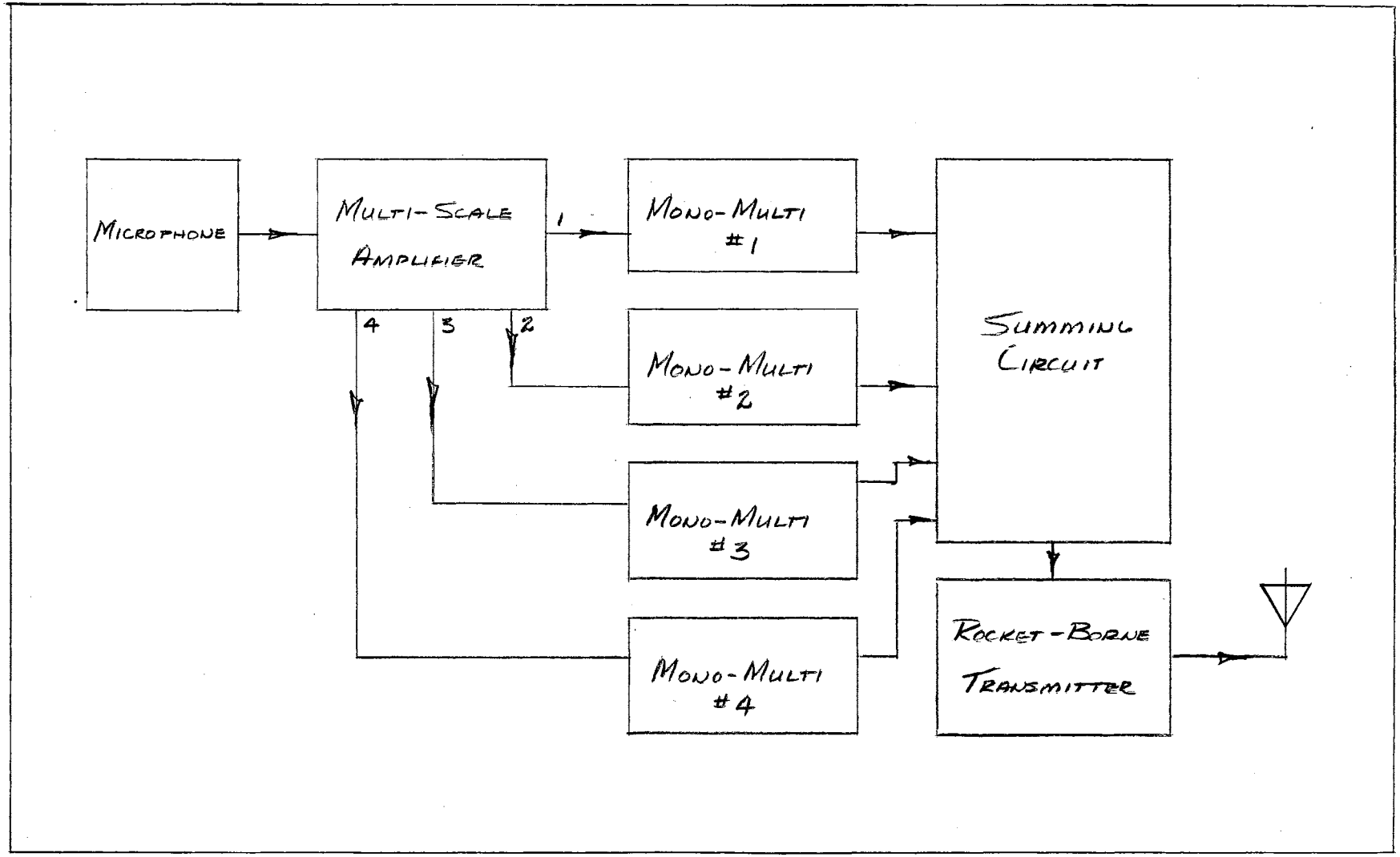

Figure 5. Multi-Scale Micrometeor Detection System.

to four scales of momentum sensitivity for each amplifier and logic circuit combination.

The use of the digital-type system simplified considerably the task of reading out the telemetry records. Pulses on the telemetry film showed the time of occurrence of the meteoric impact, with the magnitude of the pulse indicating the range of momentum in which the momentum of the incident particle was located.

A description of a single micrometeor detection system cannot be applied to all the flights, because new ideas were incorporated into the circuits between various flights. Also, the basic logic to be performed by the circuits occasionally changed between flights, necessitating revisions in the amplifier and logic circuits. In view of the various circuit revisions effected, one must, however, emphasize that in every case of revision, an effort was made to obtain the simplest workable system possible. Such an approach to the problem of instrumentation helped to minimize the possibility of circuit failures in flight. No failure to gather data on the influx of micrometeors can be attributed entirely to the failure of only the micrometeor detection system on any of the flights made so far.

The block diagram of a more elaborate digital-type micrometeor detection system is shown in Figure 6. This circuit was designed and constructed by the author as a prototype model of units for use in lunar probes launched by the United States. The unit contains twenty-two transistors, nine semiconductor diodes, and numerous miniature resistors and capacitors. The amplifier and logic circuit combination operates on only about four milliamperes of current at five volts. The unit is capable of performing logic on information supplied by three input channels

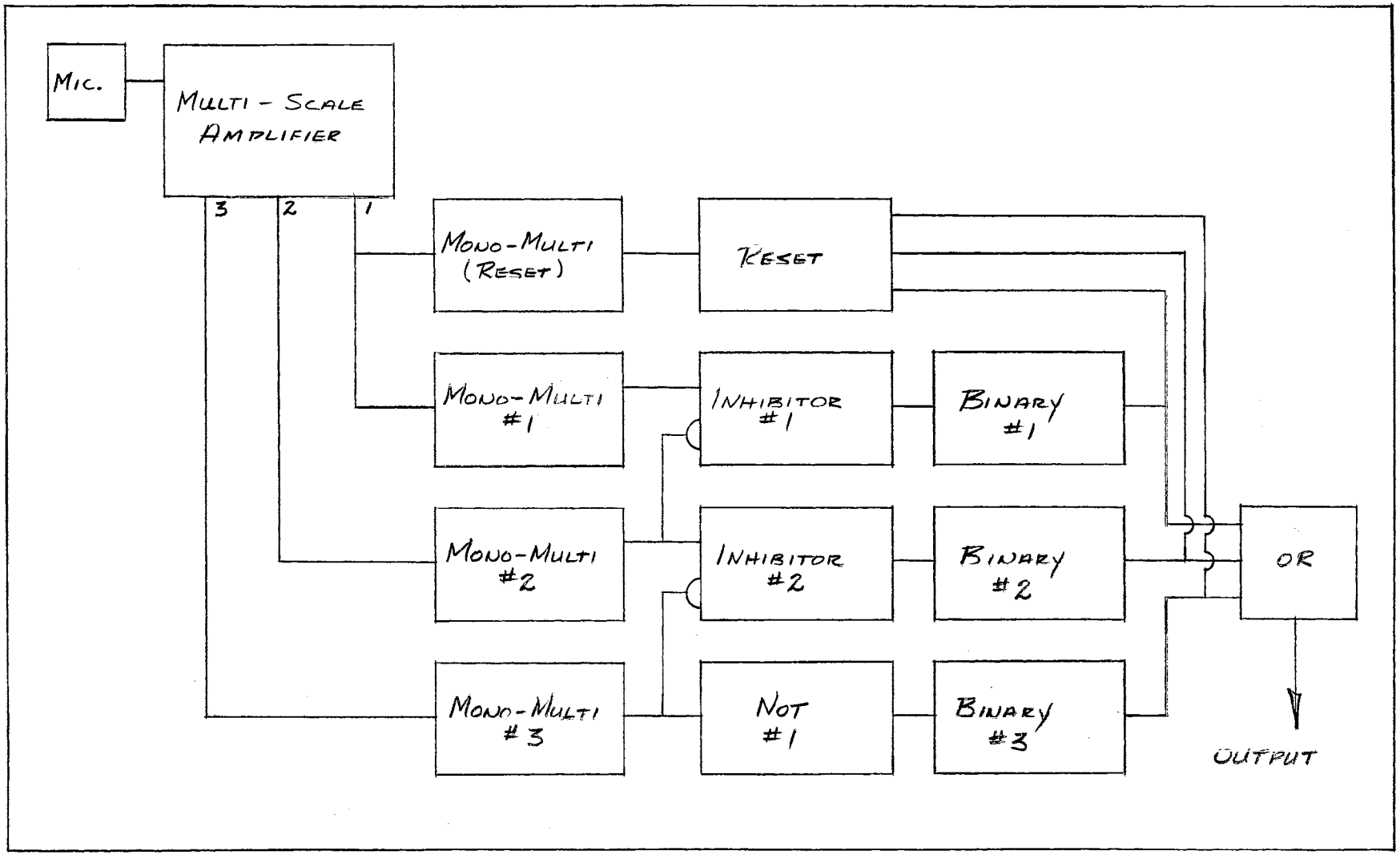

Figure 6. Proto-type Model of a Micrometeor Detection System for Space Vehicles.

with the output information of the logic circuit appearing on a single channel in a form suitable for telemetry to a ground receiving station. The low power requirements and small weight of such units are in support of the feasibility of having micrometeor detection systems mounted on virtually all vehicles that ascend to heights of 100 kilometers and higher.

CHAPTER VI

CALIBRATION OF EQUIPMENT

A realistic calibration of an acoustical type micrometeor detection system is quite difficult to perform in the laboratoy. The micrometeors that the system must be able to detect have masses of the order of 10^{-10} gm and average geocentric velocities of about 40 kilometers per second. A realistic calibration would conceivably necessitate placing the entire instrument section of a rocket into a vacuum chamber evacuated to less than about 10^{-4} cm of Hg. The pressure in the chamber would need to be low, because the pressure at 100 kilometers altitude is only about 0.5×10^{-4} cm of Hg. Particles with masses corresponding to the micrometeoric masses would then be fired against the rocket skin at velocities of about 40 kilometers per second. A feeling for the magnitude of a speed of 40 kilometers per second may be gained by noting that such a speed is more than 100 times the speed of sound in air at STP. The output voltage of the amplifier would be determined as a function of the momentum of the incident particles, and the calibration procedure would be complete. For such a calibration techniques, the momentum of the calibration particle must be known quite accurately.

At the present time, there are no convenient terrestrial means of giving the calibration particles velocities of the order of 40 kilometers per second. A significant advance in the production of hypervelocity particles has been made recently through the use of shaped charges.

Particles accelerated by shaped charges have velocities of the order of 5 kilometers per second. Shaped charges were used in the production of artificial meteors high in Earth's atmosphere with Aerobee #88 fired at HADC in October 1957. The artificial meteor experiment was performed under the direction of Zwicky, who had proposed the experiment several years previously. (46). The use of high velocity particles accelerated by shaped charges may very well be the first practical method of calibrating, on Earth, the micrometeor detection apparatus with high velocity particles. Even with the shaped charge method, the momenta of the projected particles may be so indeterminant as to prevent a reliable calibration. Additional knowledge about the nature of the collisions of small, hypervelocity particles would represent a significant gain from the use of the shaped charge technique.

The possibility of using a high-energy accelerating machine to accelerate small charged masses of micrometeoric size is negated quickly when one considers the fact that the kinetic energy of a mass of 10^{-10} gm moving with a velocity of 4×10^{6} cm sec^{-1} (a typical micrometeor in the region of interest) is about 10^{15} e.v. or about 800 ergs. In comparison, some of the most energetic primary cosmic rays are thought to have energies of the order of 10^{17} e.v. (47).

The next possibility for a calibration technique that might be used was the use of larger particles at lower velocities. Micrometeors incident on a rocket skin probably burn into the skin with total disintegration. In fact, several very definite micrometeor craters have been observed on the exposed portions of recovered Aerobee rockets by Yagoda (44). The more massive and lower velocity particles used in the laboratory calibration procedure merely bounce off the rocket skin. Thus, the

type of particle impact obtained in the calibration procedure is very nearly perfectly elastic, while the impacts of micrometeors on rocket skins are probably very nearly perfectly inelastic.

A calibration technique for the acoustical type micrometeor detection system was devised and refined by McCracken and Huggett as a term project. The details of the calibration procedure and the results obtained through the use of the calibration procedure on USAF Aerobee #77 have been reported in an unpublished term paper. (48). Little would be gained by repeating all the details of the calibration procedure as it was described in the term paper. However, a brief resume of the calibration technique may serve to point out some of the important features of the micrometeor detection system and its mode of operation.

The first method of calibrating the equipment instrumentated at OSU involved dropping small crystals of NaCl vertically onto the rocket skin. The average mass of the crystals of salt was determined by counting out and weighing a sample of salt crystals. The momentum of a crystal of salt upon impact could be determined once the mass of the crystal and the height from which the crystal was dropped were known.

If the impact of a calibration particle on the rocket skin is perfectly elastic, the impulse delivered to the rocket skin by the incident particle is just twice the momentum of the particle just before impact. Salt crystals are cubic in form, and hence even an approximation to a perfectly elastic collsions is quite difficult to obtain. The salt crystals served sufficiently well as calibration particles during the construction and testing of the micrometeor detection system. The salt was abandoned in favor of oil-well fracturizing sand before the final stages of calibration were reached.

Frac sand is a well-rounded grade of sand of fairly uniform size. A supply of frac sand was processed through a grader to sort the sand into different sizes. The grains of frac sand were far from spherical, but they represented a considerable improvement over the cubical NaCl crystals. An assistant in charge of dropping the grains of sand onto a rocket skin could, with reasonable care, sort out the sand particles according to size and shape during the particle dropping session. The assistant wore a 7x eyepiece while dropping sand and could thus avoid dropping the off-shape particles. The size of sand that proved to be most usable in the calibration procedures corresponded to a mass of about 85 μgm.

The frac sand had been in use for only a short time before a supply of small Darex glass beads was discovered. The beads were of the type commonly used in filtration experiments. The glass beads were remarkably spherical in shape and were available in several different sizes. Off-shape beads(egg-shaped, dumb-bell, etc) could be avoided quite easily during the bead dropping session. The glass beads are still in use as the calibration particles for vehicles instrumentated at OSU. The beads have been categorized according to mass, with the masses having been determined fairly well through repeated weighings of significant samples of beads. The beads were counted out into groups of 50 to 100 beads, and each group was then weighed on a sensitive analytical balance. A recent improvement in the technique of grading the beads has resulted in a better categorization of the beads according to their masses. Masses of 5 μgm, 12 μgm, 85 μgm, and 300 μgm are typical of the beads used in the calibration of a micrometeor detection system. The beads are cleaned well in order to insure more nearly elastic impacts.

The next parameter needed in the calibration procedure was the coefficient of restitution for glass beads against the impact-sensitive area of the rocket. A stainless steel diaphragm such as the one used in the nose of an Aerobee rocket was carefully leveled. Beads were dropped vertically onto the diaphragm, and the heights to which the beads rebounded were recorded. The height from which the beads were dropped was known. A knowledge of the various parameters allowed the coefficient of restitution for the beads against the stainless steel diaphragm to be computed. The experimentally determined coefficient of restitution was found to be

$$0.77 \leq \epsilon \leq 0.89$$

with $\epsilon=0.83$ being the average value.

The skins of the Aerobee rockets were made of an aluminum alloy which was almost as "alive" to particle impacts as was the stainless steel used for the diaphragms. Several beads were dropped onto the rocket skins in order to get an idea of the magnitude of the coefficient of restitution for glass beads incident on aluminum. The heights to which the beads rebounded from the aluminum were slightly less than the rebound heights for the beads incident on stainless steel, meaning that the coefficient of restitution was slightly less for the aluminum than for the stainless steel. The Cajun rockets had stainless steel skins, allowing the use of the coefficient of restitution that had been determined previously. The value of $\epsilon=0.8$ was used in all calibrations because this value seemed to be a reasonably valid approximation that could be used for all the vehicles.

Once the coefficient of restitution for the beads, the masses of the beads, and the heights from which the beads were dropped were known,

the impulse delivered to the rocket skin by an incident particle could be computed. Proper choice of the mass and dropping height for the beads resulted in impulses comparable in magnitude to those delivered to the rocket skin by micrometeors traveling with hypervelocities. For example, a 25 μgm bead dropped from a height of 5 cm onto the diaphragm produced an impulse about equal to that which would be produced by a micrometeor of mass 1.25×10^{-9} gm incident with a velocity of 40 kilometers per second. An impulse of comparable magnitude would also be produced in the collision of a rocket moving at 1 kilometer per second with a stationary particle of about 10^{-8} gm mass. Again, mention is made of the fact that the laboratory calibration involves almost perfectly elastic impacts, while under actual flight conditions, the collisions of micrometeors with the rocket are probably completely inelastic.

A check was made early in the calibration procedure to be sure that the calibration particles were falling like a small projectile moving at low velocity through a viscous fluid rather than like a particle behaving according to kinetic theory. The diameter of a typical calibration particle is about 10^{-2} cm, while the mean free path in air for laboratory conditions is about 10^{-5} cm, several orders of magnitude less than the diameter of the calibration particles. Care had to be exercised in the choice of the dropping height for a given size of bead, for the beads reach terminal velocities as predicted by Stoke's law. The subject of terminal velocities and the choice of a maximum dropping height for a given size of bead are treated more fully in Appendix C. Some of the smallest beads used in the calibration procedure reach terminal velocities in only a few millimeters of descent distance. Also, larger beads should not be dropped from small heights because of the

indeterminancy in the dropping height. One can tell quite easily, from the response of the micrometeor detection system, whether the calibration particles are traveling at their terminal velocities.

An alternate calibration technique would be that of dropping the beads from such heights that the difference between the velocity of a bead just before impact and the terminal velocity for the bead would be negligible. Disadvantages of this technique are the difficulty in hitting the rocket skin in the desired area, indeterminancy in the angle of incidence of the bead on the rocket skin, and the large heights from which the fairly massive calibration beads must be dropped in order that they attain their terminal velocities. In view of these difficulties, the technique involving impact velocities that were small in comparison to the terminal velocities was chosen and used throughout the calibration procedures followed at OSU.

The impulses delivered to the rocket skin by the incident particles serve as signals for the crystal microphone placed in contact with the rocket skin. The output of the microphone is amplified by a high-gain transistorized amplifier and appears as a pulse at the output of the amplifier. Calibration of the earlier micrometeor detection systems consisted of dropping beads and measuring the output of the amplifier in volts. A plot of output voltage as a function of impulse constituted the calibration curve. For perfectly inelastic collsions, the impulse is just equal to the momentum of the incident particle, so the coordinates of the calibration curve could be labeled as amplifier output voltage and micrometeor momentum. A calibration curve labeled in such a manner is then used as the calibration curve for the actual flight conditions.

The calibration procedure used for the later flights, which were equipped with the digital type systems, was considerably simplified over the procedure used for the earlier flights. A typical system had four scales of momentum sensitivity covering the region of interest for micrometeoric particles. Only the "break points" between the scales had to be located during the calibration. A break point could be located roughly by dropping only about a dozen beads. The careful choice of bead mass and dropping height then allowed the break point to be located quite accurately.

CHAPTER VII

EXPERIMENT DATA

Data were relayed from the rocket-borne micrometeor detection systems to the ground by means of a telemetry link between the rocket and ground. The modulated radio wave transmitted from the rocket was received by ground receiving stations. Permanent receiver installations were used to receive the pulse-time telemetry signal, while portable units operated by OSU personnel were used to receive the FM-FM telemetry signal.

Amplification and demodulation of the received telemetry signal transformed the signal into a form suitable for display on a cathode ray oscilloscope. The waveforms displayed on the CRO were then recorded photographically, with the processed telemetry film serving as a permanent record of the micrometeor data from the various rocket flights.

The type of information that was recorded on the telemetry film is shown in the sketches of Figure 7. The sketches illustrate sections of telemetry film, with the pulses shown being typical of those appearing on the actual telemetry film.

The telemetry film was read out as soon as possible after each rocket flight. The telemetry films all showed a multitude of pulses during the rocket's upward passage through the atmosphere. Such pulses could conceivably be caused by rocket noises during powered flight, ice crystals in the atmosphere, and meteoric fragments that drift slowly down

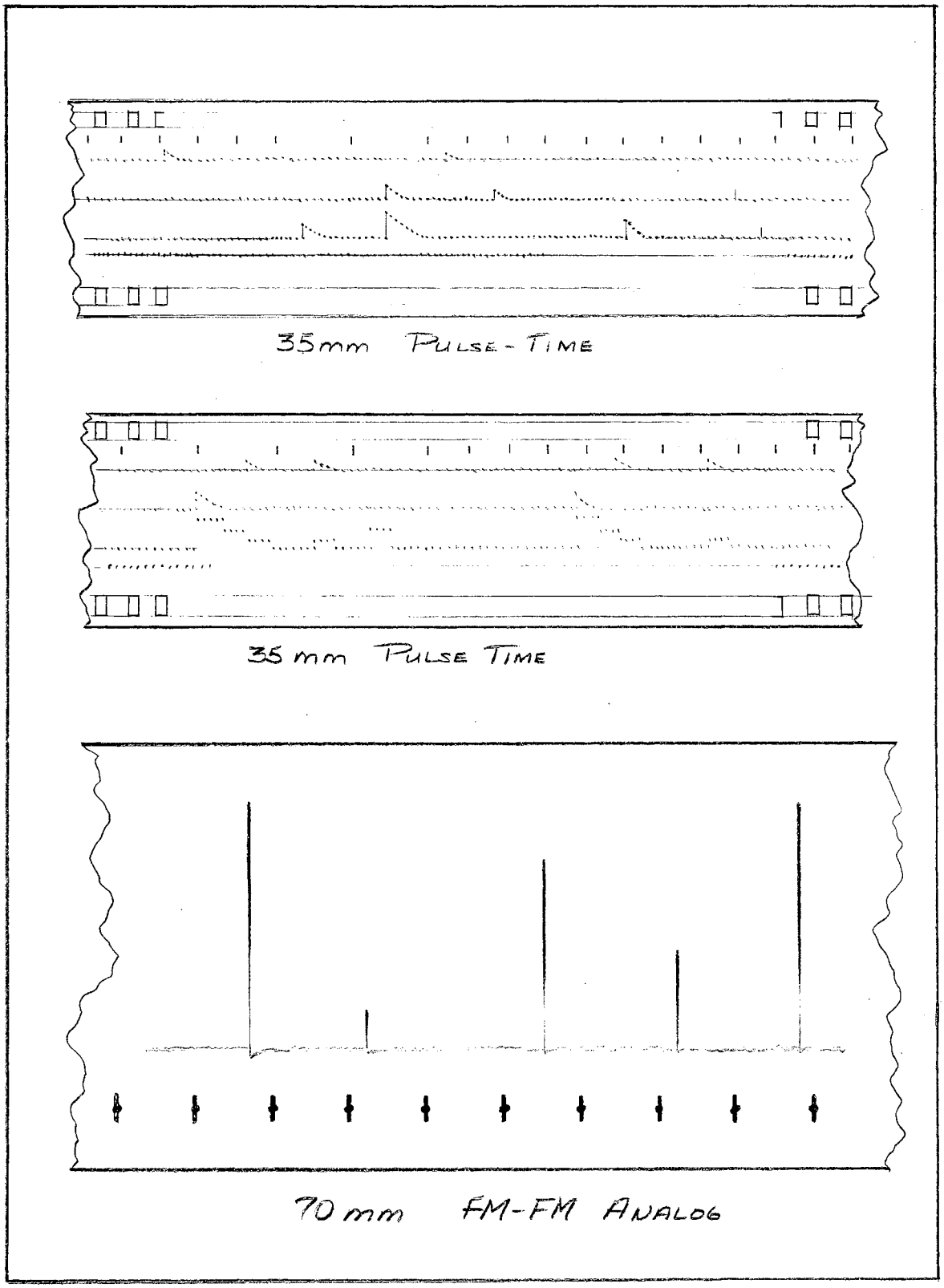

Figure 7. Sketches of Sections of Telemetry Film for the Micrometeor Experiment.

through the atmosphere. Such possible effects made evident the futility of trying to count pulses from X time (the time at which the rocket was fired). Therefore, the pulse count was begun at a time such that the pulses seemed to represent intelligible information. The minimum starting time for pulse counts corresponded, on all flights except AA6.202, to an altitude of less than 100 kilometers. The read-out pulses were arranged in tabular form according to their time of occurrence and magnitude. Any pulses that could be immediately attributed to causes within the rocket or telemetry system were dropped from the list.

The remaining task, that of determining which of the pulses could be associated with micrometeoric impacts, has proven to be one of the more difficult parts of the data analysis. Each flight had its own peculiarities, necessitating the use of different techniques of analysis for each of the various flights. Specific questions that arose during the data analysis pertained to the determination of a minimum height above which the micrometeor count could be considered as reliable, whether to include in the count the bursts of quite closely spaced impacts, and how to choose a minimum allowable pulse spacing or "dead time" for the system.

The first of the three questions presented in the preceding paragraph was answered by considering the deceleration of meteoric particles upon entering Earth's atmosphere. Grimminger had treated the problem of deceleration using the atmospheric densities, pressures, and scale heights available in 1947. The use of Rocket Panel (12) values for the atmospheric parameters leads to results that are probably more acceptable for recent work. An even later set of values for the atmospheric parameters has been determined from high-altitude rocket measurements at

White Sands Proving Ground and at Fort Churchill by Horowitz and LaGow (13, 14). The values given by Rocket Panel and Horowitz and LaGow do not lead to widely divergent results for the region of maximum deceleration of the micrometeors. The quantitative aspects of the deceleration of the micrometeors by the atmosphere have been considered in greater detail in Appendix D.

Consideration of the deceleration of a 1.25×10^{-10} gm micrometeor led to the choice of 100 kilometers as the minimum height at which the pulse count should be started. A 1.25×10^{-10} gm micrometeor of density 3.6 gm cm^{-3} entering vertically into the atmosphere has been decelerated by the time it reaches an altitude of 100 kilometers until the velocity of the micrometeor is only 0.85 of the original geocentric velocity. Thus, the momentum has already changed by 15% at the time the micrometeor reaches 100 kilometers. Only 5 to 10 additional kilometers of descent are required to reduce the velocity of the micrometeor to a negligibly small value.

Bursts of impacts have occurred on several flights, forming the basis for the second question that arose in the analysis of the flight data. The origin of these bursts is not known, and although the inclusion of these bursts in a total count of micrometeors may seem inadvisable, the bursts are left in the total count. In no case, does the omission of a burst decrease the influx rate for that scale of momentum sensitivity by more than a factor of 2.5.

The third and remaining major question arising in the data analysis was that of determining a minimum time by which one pulse could follow a previous pulse and still be considered as reliable. All of the vehicle skins except that of the Spaerobee were quite "alive" to the impact of

the calibration beads. How the skins will respond to the impact of hypervelocity particles cannot be easily inferred from the response of the skin to a low velocity calibration bead. The microphone, amplifier, and pulse-shaping network, as a combination, had dead times of the order of a few milliseconds, at a maximum. However, oscilloscopic displays of the output voltage of the pulse-shaping network have shown, for skin-mounted microphones, an effect similar to that which might be caused by sustained ($\sim$0.8 seconds) acoustical disturbances in the skin. This "ringing" effect has not been investigated to any extent, because the results of such an investigation would probably not be of much significance until more is known about the relative characteristics of the collisions of calibration and hypervelocity particles.

Influx rates were computed for each flight after omitting the second pulse of any pair of pulses with a separation of less than 0.5 second for the Aerobee flights and of less than 0.8 second for the Cajun and Spaerobee flights. In one case, the influx rate obtained through consideration of the minimum pulse separation differed from the original value of influx by a factor of 5; in another case, the rates differed by a factor of 3, and in two other cases, the influx dropped to zero upon omission of the closely spaced pulses. The remainder of the influx rates remained almost unchanged upon omission of the closely spaced pulses.

The above paragraphs, in which the three major questions arising in the analysis of the flight data are discussed, show that no justifiable changes in the method of analysis seem to change the influx rates by an appreciable amount. The two cases in which the influx rates dropped to zero upon omission of closely spaced pulses had influx rates that were

based on low values of particle count. Thus, these particular particle counts could have been of rather low statistical reliability, and the dropping to zero of two of the influx rates upon application of a more stringent analysis should not be viewed with a too great concern.

The quantitative data obtained through the processes of analysis outlined in the preceding paragraphs may now be presented. The first influx data presented is that based on the total particle count. The influx data for each flight is presented, together with other pertinent information for the flight, in Tables II through VIII.

The information given Tables II through VIII constitute the available data for seven separate vehicles. More than one set of data is available for each of several of the vehicles, because some of the vehicles had more than one impact-sensitive surface available, and the majority of the micrometeor detection systems had more than one scale of momentum sensitivity for each microphone-amplifier combination.

Influx rates, calculated on the basis of the total count for each of the scales of momentum sensitivity, are presented in tabular form in Table IX. Elimination of the bursts from the total counts leads to the influx rates shown in Table X. Omission of all pulses separated by less than 0.5 second for the Aerobee flights and by less than 0.8 second for the Cajun and Spaerobee flights reduced the influx rates shown in Table IX to the values shown in Table XI. The data of Tables IX, X, and XI are shown, in graphical form, in Figures 8, 9, and 10, respectively.

The influx rates listed in Table IX represent the maximum influx rates that can be obtained from the available data, provided that the effective areas used in the computations of the influx rates are correct. The effective areas used are those designated by Dubin.

The influx rates shown in Table X are either unchanged or are lower than those of Table IX. The influx rates of Table XI represent about the lowest values obtainable from the existing data. The changes in datum points that occur when the extreme methods of analysis are applied are illustrated in Figure 11. The influx rates from both Table IX and Table XI are plotted as a function of particle momentum in Figure 11. Several of the datum points remain unchanged under the different analyses, while two of the datum points based on total count disappear when the minimum pulse separation condition is imposed. The remainder of the datum points shift by varying amounts, with the largest shifts being associated with the higher momentum particles where the influx rates are probably of lowest statistical reliability. Datum points representing the influx rates obtained from the same data under different methods of analysis are joined ( ), in Figure 11, where graphically possible. The joined datum points are not intended to convey the meaning of a probable deviation; the points are joined only to show the limits of the range over which the influx rate can be varied by application of the different methods of analysis.

No particular attempt has been made to apply methods of statistical analysis to the data, because the sampling times on all vehicles except Explorer I have been rather short (~100 to 200 seconds). Also, the number of impacts used for some of the influx rates was so small (2 impacts per flight per momentum scale in some cases) as to make the statistical reliability of these influx rates doubtful.

TABLE II

FLIGHT DATA

Vehicle:	USAF Aerobee #80
X time:	0630 MST, 16 July 1957
Launch site:	HADC, New Mexico
Zenith altitude:	128 kilometers
Data gathering time:	129 seconds
Effective area:	0.5 m^2 (skin)
	0.05 m^2 (diaphragm)

Scale	Sensitivity $\frac{gm\ cm}{sec}$	Impacts	Influx $\frac{particles}{m^2\ sec}$
S_1 (skin)	2.4×10^{-3}	8	0.124
S_2 (skin)	5.0×10^{-3}	10	0.155
S_1 (diaphragm)	7.0×10^{-4}	48	7.45
S_2 (diaphragm)	5.0×10^{-3}	17	2.64
S_3 (diaphragm)	3.0×10^{-2}	10	1.55

Comments:

A burst of 3 pulses occurred at X + 234.5 seconds for the skin system, and a burst of 6 pulses occurred between X + 232.4 and X + 234.6 seconds for the diaphragm. The pulses of the burst on the skin system were spaced about 20 milliseconds apart.

TABLE III

FLIGHT DATA

Vehicle:	USAF Aerobee #88
X time:	2212 MST, 16 October 1957
Launch site:	HADC
Zenith altitude:	113 kilometers
Data gathering time:	100 seconds
Effective area:	0.5 m^2 (skin)
	0.05 m^2 (diaphragm)

Scale	Sensitivity $\frac{gm\ cm}{sec}$	Impacts	Influx $\frac{particles}{m^2\ sec}$
S_1 (skin)	6.0×10^{-4}	33	0.66
S_2 (skin)	1.5×10^{-3}	2	0.04
S_1 (diaphragm)	7.0×10^{-4}	7	1.4

TABLE IV

FLIGHT DATA

Vehicle:	Explorer I ($\propto$1958)
X time:	0355 GCT, 1 February 1958
Launch site:	Cape Canaveral, Florida
Data gathering time:	2.09×10^4 seconds
Effective area:	0.0725 m^2

Scale	Sensitivity $\frac{gm\ cm}{sec}$	Impacts	Influx $\frac{particles}{m^2\ sec}$
S_1 (skin)	2.5×10^{-3}	45	0.03

TABLE V

FLIGHT DATA

Vehicle:	USAF Cajun AA6.202
X time:	0533 MST, 1 May 1958
Launch site:	HADC
Zenith altitude:	136 kilometers
Data gathering time:	163 seconds
Effective area:	0.2 m^2

Scale	Sensitivity $\frac{gm\ cm}{sec}$	Impacts	Influx $\frac{particles}{m^2\ sec}$
S_1	6.0×10^{-4}	26	0.80
S_2	1.8×10^{-3}	26	0.80
S_3	5.0×10^{-2}	12	0.37

Comments:

A burst of 6 pulses occurred between X + 254.3 and X + 256.7 seconds.

The pulse count was begun at X + 126.6 seconds, after the thermally initiated pulses had slowed down.

TABLE VI

FLIGHT DATA

Vehicle:	USAF Cajun AA6.203
X time:	2200 CST, 15 October 1958
Launch site:	Fort Churchill, Manitoba, Canada
Zenith altitude:	150 kilometers
Data gathering time:	199 seconds
Effective area:	0.2 m^2

Scale	Sensitivity $\frac{gm\ cm}{sec}$	Impacts	Influx $\frac{particles}{m^2\ sec}$
S_1	2.5×10^{-4}	77	1.93
S_2	7.0×10^{-4}	39	0.98
S_3	1.2×10^{-3}	2	0.05
S_4	3.0×10^{-3}	3	0.075

TABLE VII

FLIGHT DATA

Vehicle:	USAF Cajun AA6.204
X time:	0600 CST, 14 October 1958
Launch site:	Fort Churchill, Manitoba, Canada
Zenith altitude:	136 kilometers
Data gathering time:	173 seconds
Effective area:	0.2 m^2

Scale	Sensitivity $\frac{gm\ cm}{sec}$	Impacts	Influx $\frac{particles}{m^2\ sec}$
S_1	3.0×10^{-4}	48	1.37
S_2	1.2×10^{-3}	2	0.058

TABLE VIII

FLIGHT DATA

Vehicle:	USAF Spaerobee AA10.01
X time:	1047 CST, 22 October 1958
Launch site:	Fort Churchill, Manitoba, Canada
Zenith altitude:	176 kilometers
Data gathering time:	208 seconds
Effective area:	0.04 m^2

Scale	Sensitivity $\frac{gm\ cm}{sec}$	Impacts	Influx $\frac{particles}{m^2\ sec}$
S_1	9.0×10^{-4}	29	3.5
S_2	0.12	2	0.024

Comments:

The Sparrow motor was not allowed to fire because of range safety, resulting in a lower zenith altitude than expected.

TABLE IX

COMPOSITE FLIGHT DATA

Influx Rates Obtained by Using All Pulses

Vehicle	Scale	Momentum Sensitivity $\left(\frac{gm\ cm}{sec}\right)$	Influx $\left(\frac{particles}{m^2\ sec}\right)$
Aerobee #80	S_1 (skin)	2.4×10^{-3}	0.12
	S_2 (skin)	5.0×10^{-3}	0.16
	S_1 (diaphragm)	7.0×10^{-4}	7.45
	S_2 (diaphragm)	5.0×10^{-3}	2.64
	S_3 (diaphragm)	3.0×10^{-2}	1.55
Aerobee #88	S_1 (skin)	6.0×10^{-4}	0.66
	S_2 (skin)	1.5×10^{-3}	0.04
	S_1 (diaphragm)	7.0×10^{-4}	1.4
Explorer I	S_1	2.5×10^{-3}	0.03
Cajun AA6.202	S_1	6.0×10^{-4}	0.80
	S_2	1.8×10^{-3}	0.80
	S_3	5.0×10^{-2}	0.37
Cajun AA6.203	S_1	2.5×10^{-4}	1.93
	S_2	7.0×10^{-4}	0.98
	S_3	1.2×10^{-3}	0.05
	S_4	3.0×10^{-3}	0.075
Cajun AA6.204	S_1	3.0×10^{-4}	1.37
	S_2	1.2×10^{-3}	0.058
Spaerobee AA10.01	S_1	9.0×10^{-4}	3.5
	S_2	1.2×10^{-1}	0.024

TABLE X

COMPOSITE FLIGHT DATA

Influx Rates Obtained Upon Eliminating Bursts

Vehicle	Scale	Momentum Sensitivity $\left(\frac{\text{gm cm}}{\text{sec}}\right)$	Influx $\left(\frac{\text{particles}}{\text{m}^2 \text{ sec}}\right)$
Aerobee #80	S_1 (skin)	2.4×10^{-3}	0.12
	S_2 (skin)	5.0×10^{-3}	0.11
	S_1 (diaphragm)	7.0×10^{-4}	7.45
	S_2 (diaphragm)	5.0×10^{-3}	2.64
	S_3 (diaphragm)	3.0×10^{-2}	0.62
Aerobee #88	S_1 (skin)	6.0×10^{-4}	0.66
	S_2 (skin)	1.5×10^{-3}	0.04
	S_1 (diaphragm)	7.0×10^{-4}	1.4
Explorer I	S_1	2.5×10^{-3}	0.03
Cajun AA6.202	S_1	6.0×10^{-4}	0.80
	S_2	1.8×10^{-3}	0.80
	S_3	5.0×10^{-2}	0.18
Cajun AA6.203	S_1	2.5×10^{-4}	1.93
	S_2	7.0×10^{-4}	0.98
	S_3	1.2×10^{-3}	0.05
	S_4	3.0×10^{-3}	0.075
Cajun AA6.204	S_1	3.0×10^{-4}	1.37
	S_2	1.2×10^{-3}	0.058
Spaerobee AA10.01	S_1	9.0×10^{-4}	3.5
	S_2	1.2×10^{-1}	0.024

TABLE XI

COMPOSITE FLIGHT DATA

Influx Rates Obtained by Dropping Closely Spaced Pulses

Vehicle	Scale	Momentum Sensitivity $\left(\frac{gm\ cm}{sec}\right)$	Influx $\left(\frac{particles}{m^2\ sec}\right)$
Aerobee #80	S_1 (skin)	2.4×10^{-3}	0.11
	S_2 (skin)	5.0×10^{-3}	0.09
	S_1 (diaphragm)	7.0×10^{-4}	6.01
	S_2 (diaphragm)	5.0×10^{-3}	1.86
	S_3 (diaphragm)	3.0×10^{-2}	0.31
Aerobee #88	S_1 (skin)	6.0×10^{-4}	0.58
	S_2 (skin)	1.5×10^{-3}	0.04
	S_1 (diaphragm)	7.0×10^{-4}	1.4
Explorer I	S_1	2.5×10^{-3}	0.03
Cajun AA6.202	S_1	6.0×10^{-4}	0.58
	S_2	1.8×10^{-3}	0.52
	S_3	5.0×10^{-2}	0.12
Cajun AA6.203	S_1	2.5×10^{-4}	1.68
	S_2	7.0×10^{-4}	0.58
	S_3	1.2×10^{-3}	0.05
	S_4	3.0×10^{-3}	0.0
Cajun AA6.204	S_1	3.0×10^{-4}	1.04
	S_2	1.2×10^{-3}	0.06
Spaerobee AA10.01	S_1	9.0×10^{-4}	2.4
	S_2	1.2×10^{-1}	0.0

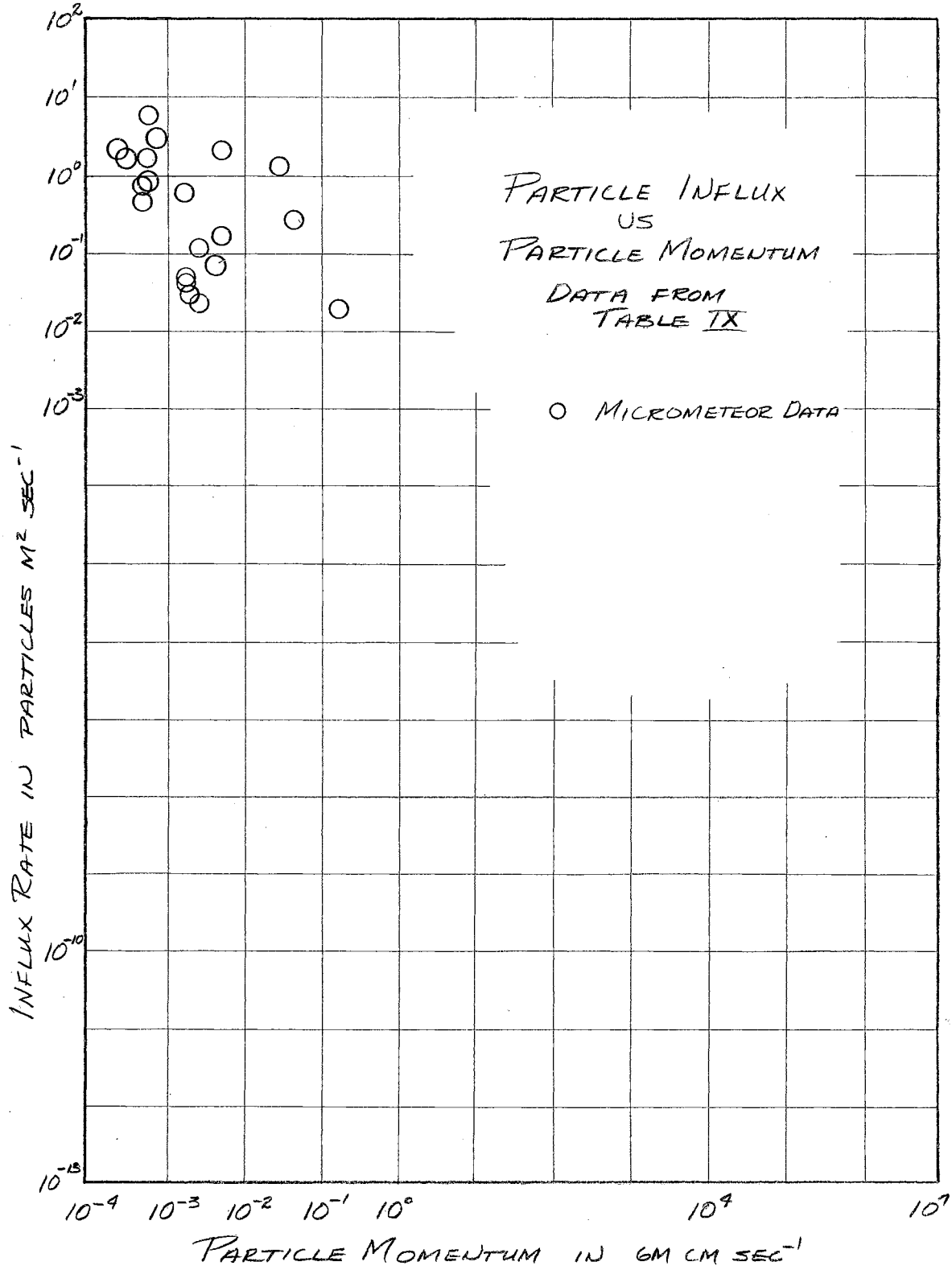

Figure 8. Measured Micrometeor Influx Rates (Data from Table IX).

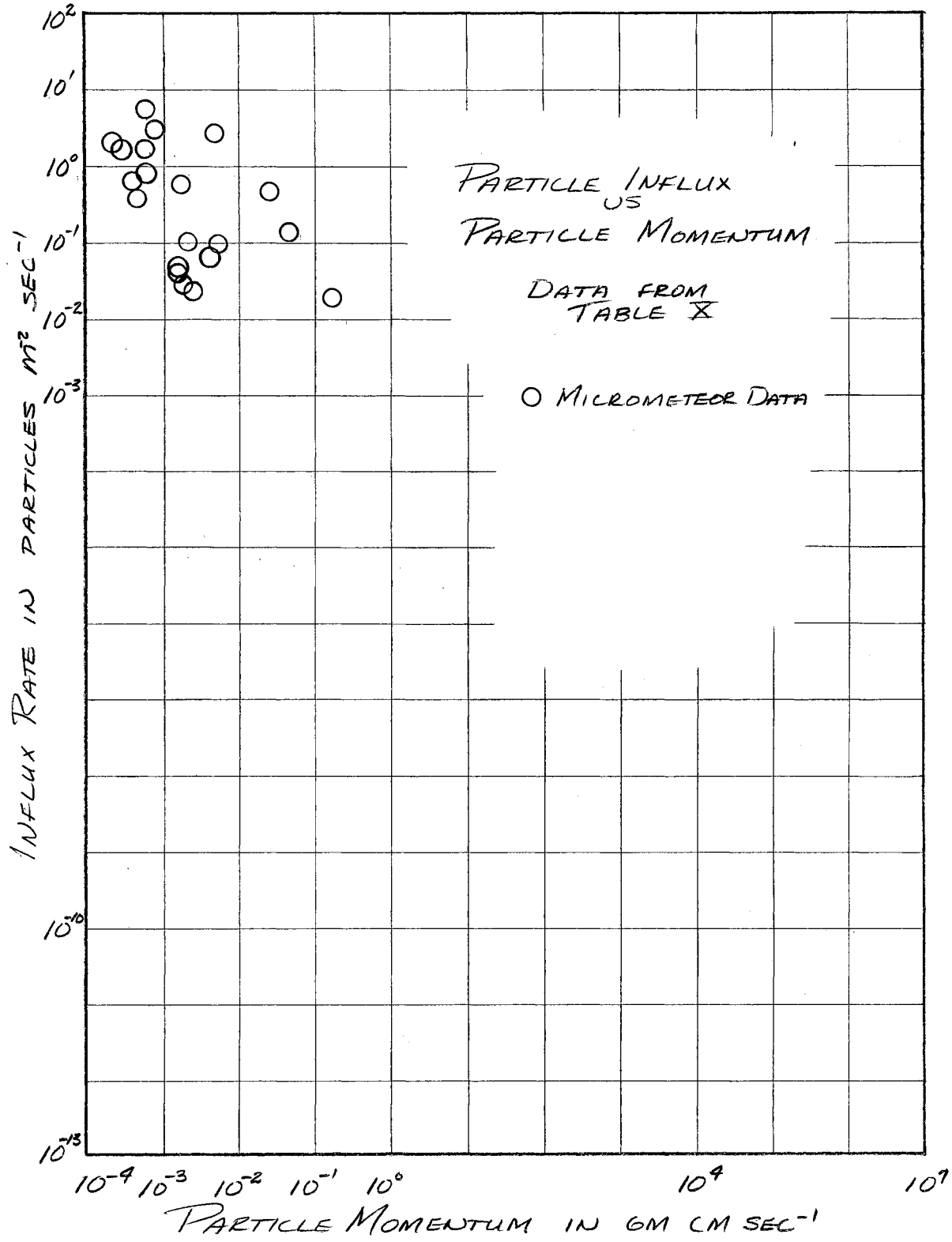

Figure 9. Measured Micrometeor Influx Rates (Data from Table X).

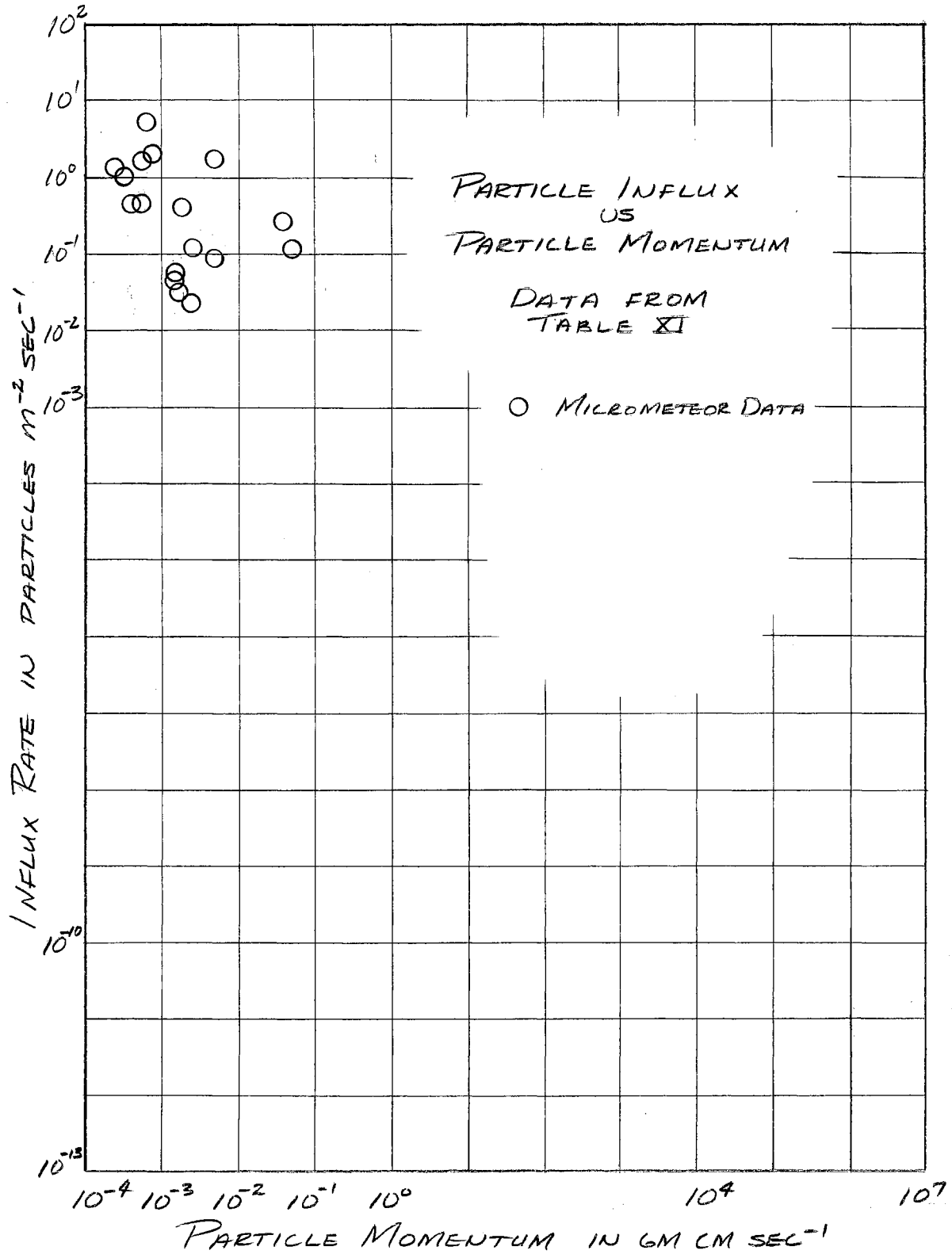

Figure 10. Measured Micrometeor Influx Rates (Data from Table XI).

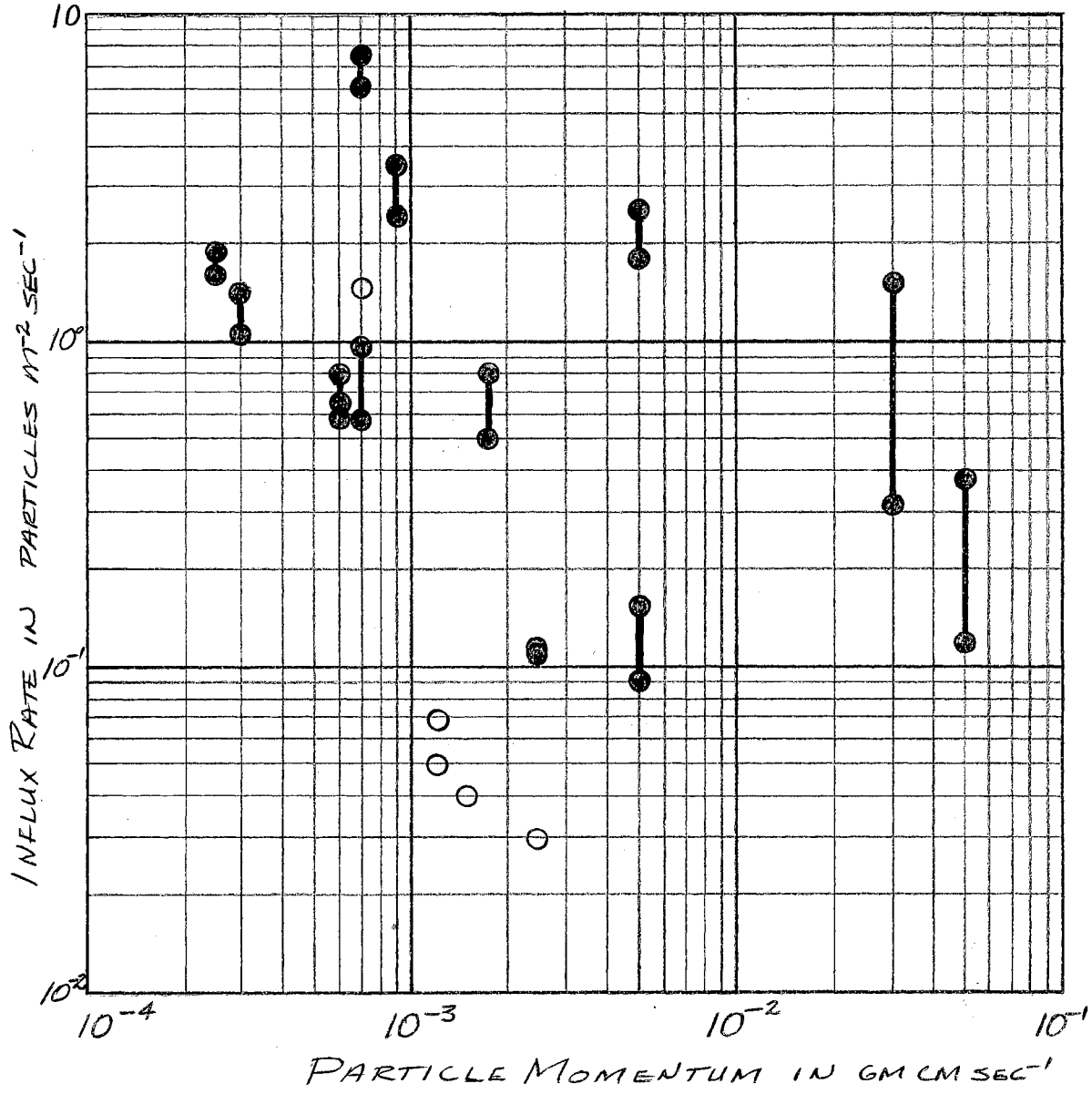

Figure 11. Variation of the Influx Rates under Extreme Analyses.

CHAPTER VIII

INFLUX DATA FROM OTHER SOURCES

Russian Micrometeor Data

The micrometeor influx rates based on the information gathered by Sputnik I have been reported by Nazarova (38). Short period increases in the micrometeor influx rate were observed at several altitudes during the movement of the satellite. The high influx rates and the altitudes at which they occurred are shown in Table XII.

TABLE XII

MICROMETEOR INFLUX RATES FOR SPUTNIK I

Altitude (Km)	Influx Rate $\left(\frac{\text{particles}}{m^2 \text{ sec}}\right)$
500 to 600	38 ± 10
1300 to 1500	40 ± 18
1700 to 1800	90 ± 34

The influx rates listed in Table XII are the influx rates that were reported at the International Astronomical Union Meeting in Moscow during August, 1958. (34).

The average micrometeor influx rate, as given in Nazarova's (38) paper, was less than 0.01 counts per second on a surface of 840 cm^2. In reduced form, this influx rate would be less than 0.1 particle m^{-2} sec^{-1}. The system sensitivity was given as 0.1 to 10^{-3} gm cm sec^{-1} in

one section of the report and as 4×10^{-3} gm cm sec^{-1} in another section of the report. The micrometeor influx rate of 0.1 particle m^{-2} sec^{-1} compares quite favorably with the influx rate measured on Explorer I. Therefore, an influx rate of 0.1 particle m^{-2} sec^{-1} at a momentum sensitivity of 4×10^{-3} gm cm sec^{-1}, as reported by Nazarova (38) for Sputnik I, is taken as a usable datum point for use in the composite analysis of Chapter IX. The other influx rates given by Nazarova are considerably higher than any influx rates ever obtained by the group at OSU.

Data from Considerations of Zodiacal Light

Some of the theoretical aspects of zodiacal light have been treated by van de Hulst (15) and by Beard (49). The work of van de Hulst does not yield a datum point that is usable in Chapter IX because his attention seems to have been directed toward particles of telescopic meteor size. The space density of particles of the telescopic meteor range, as determined by van de Hulst, was 10^4 higher than expected. If the particles most effective in producing zodiacal light are smaller than radar meteors, then the radii of the particles considered by van de Hulst are several orders of magnitude too large.

Beard (49) has recently published a theoretical treatment of zodiacal light. The particles thought to be most effective in producing the zodiacal light have radii of 1μ to 5μ, according to the article. Beard obtains a space density of 10^{-14} to 10^{-15} particles cm^{-3} along Earth's orbit for particles of 1μ to 5μ radius. The space density of particles in the immediate neighborhood of Earth may be somewhat higher, perhaps 10^{-10} to 10^{-11} particles cm^{-3}, because of a "gathering" effect on the small particles of the solar system. (49).

In order to obtain a datum point from the values given by Beard, we assume that a particle of radius 5μ and density 3.6 gm cm^{-3} is the most effective size in producing zodiacal light. Such a particle has a mass of 2×10^{-9} gm and an average geocentric momentum of 8×10^{-3} gm cm sec^{-1}. Assumption of a space density of particles of 10^{-13} particles cm^{-3} at typical rocket altitudes leads to an influx rate of 4×10^{-3} particles m^{-2} sec^{-1} for particles of 8×10^{-3} gm cm sec^{-1} momentum, which may be considered as a usable datum point for the composite analysis of Chapter IX.

Siedentopf (18) has found that the interplanetary particles have, for the most part, radii less than 100μ. Radiation pressure is effective in removing particles of less than about 1μ in diameter from the solar system. The particles with radii of 1μ to 100μ are quite likely metallic particles. Seidentopf concludes that the particles most effective in producing zodiacal light probably have radii of the range of 1μ to 100μ.

The average value for radii on the range 1μ to 100μ would be 50μ. However, in choosing a typical value for the radius of the particles most effective in producing the zodiacal light, one should remember that the new mass distribution function will predict a preponderance of particles with radii closer to 1μ than to 100μ. A value of 10μ for the radius of a typical particle seems to be a reasonable choice. A particle of 10μ radius and 3.6 gm cm^{-3} density has a mass of about 1.5×10^{-8} gm and an average geocentric momentum of 0.06 gm cm sec^{-1}. Seidentopf gives a space density for particles 1μ to 300μ in radius as 2.2×10^{-5} particles cm^{-3}. These numerical values may be combined to given an influx rate of 8.8×10^{-5} particles m^{-2} sec^{-1} for a

momentum sensitivity of 6×10^{-2} gm cm sec^{-1}. This influx rate is regarded as usable for the composite analysis of Chapter IX.

Allen (41) lists Takakubo's (16) estimated radius and space density at 1 A.U. of the particles most effective in producing zodiacal light as 20 μ and 5×10^{-16} particles cm^{-3}, respectively. The influx rate for these particles is 2×10^{-5} particles m^{-2} sec^{-1}. Next, the geocentric momentum of a typical particle must be determined, requiring a knowledge of the mass of the particle. The particles most effective in producing the zodiacal light are probably about 10^2 times more massive than the micrometeors detected on most rocket flights. Thus, a choice of 1 gm cm^{-3} as the density of the particles may be preferred over the choice of 3.6 gm cm^{-3} as the density. A particle of 1 gm cm^{-3} density and 20 μ radius has a mass of 3.4×10^{-8} gm and an average geocentric momentum of 0.136 gm cm sec^{-1}.

Thus, the above procedure has yielded an additional datum point for use in the composite analysis. The datum point is an influx of 2×10^{-5} particles m^{-2} sec^{-1} for a particle momentum of 0.136 gm cm sec^{-1}.

Representative Visual Meteor Data

Allen (41) gives the space density for particles of less than 0.003 gm mass as 5×10^{-23} gm cm^{-3}, with a preponderance of particles of 10 μ radius. If the density of the particles is taken as 1 gm cm^{-3}, a typical particle has a mass of 4.2×10^{-9} gm and a momentum of 0.0168 gm cm sec^{-1}. The datum point derivable from this information is an influx rate of 4.8×10^{-4} particles m^{-2} sec^{-1} for a particle momentum of 0.0168 gm cm sec^{-1}.

Watson (1) appears to have been the first to extrapolate visual meteor data out to the radiation pressure limit. The data of Table XIII has been extracted or derived from the data given by Watson (1). This set of data seems to be a fairly representative set of visual meteor data and can, therefore, be used as a kind of "reference" set of data. A set of visual meteor data presented earlier by Watson (50) is the basis for the data shown in Table XIV.

The data shown in Table XV has been derived from a set of visual meteor data presented by Lovell (51).

The particle momenta shown in Tables XIII, XIV, and XV have been based on the mass to visual magnitude relationship defined earlier in Table I and an average geocentric velocity of 40 kilometers per second. In every case, the masses of the meteors, as determined by Table I, are different from the masses specified by the original investigator.

TABLE XIII

VISUAL METEOR DATA

Based on Watson (1), Pg. 92

Visual Magnitude	Mass (gm) (Watson)	Mass (gm) (Table I)	Particle Momentum* $\left(\frac{\text{gm cm}}{\text{sec}}\right)$	Number of Meteors Incident on Earth per day	Influx Rate $\left(\frac{\text{particles}}{\text{m}^2 \text{ sec}}\right)$
-3	4	20	8×10^{7}	2.8×10^{4}	6.1×10^{-16}
-2	1.6	8	3.2×10^{7}	7.1×10^{4}	1.6×10^{-15}
-1	6.3×10^{-1}	3	1.2×10^{7}	1.8×10^{5}	3.9×10^{-15}
0	2.5×10^{-1}	1.25	5×10^{6}	4.5×10^{5}	9.8×10^{-15}
1	1.0×10^{-1}	5.0×10^{-1}	2×10^{6}	1.1×10^{6}	2.4×10^{-14}
2	4.0×10^{-2}	2.0×10^{-1}	8×10^{5}	2.8×10^{6}	6.1×10^{-14}
3	1.6×10^{-2}	8.0×10^{-2}	3.2×10^{5}	7.1×10^{6}	1.6×10^{-13}
4	6.3×10^{-3}	3.0×10^{-2}	1.2×10^{5}	1.8×10^{7}	3.9×10^{-13}
5	2.5×10^{-3}	1.75×10^{-2}	5×10^{4}	4.5×10^{7}	9.8×10^{-13}
6	1.0×10^{-3}	5.0×10^{-3}	2×10^{4}	1.1×10^{8}	2.4×10^{-12}
7	4.0×10^{-4}	2.0×10^{-3}	8×10^{3}	2.8×10^{8}	6.1×10^{-12}
8	1.6×10^{-4}	8.0×10^{-4}	3.2×10^{3}	7.1×10^{8}	1.6×10^{-11}
9	6.3×10^{-5}	3.1×10^{-4}	1.2×10^{3}	1.8×10^{9}	3.9×10^{-11}
10	2.5×10^{-5}	1.25×10^{-4}	5×10^{2}	4.5×10^{9}	9.8×10^{-11}

* The momenta are based on mass values from Table I and an average geocentric velocity of 40 Km sec^{-1}.

TABLE XIV

VISUAL METEOR DATA

Based on Watson (50), Pg. 623

Visual Magnitude		Mass (gm) (Table I)	Particle Momentum* $\left(\frac{\text{gm cm}}{\text{sec}}\right)$	Number of Meteors Incident on Earth per day	Influx Rate $\left(\frac{\text{particles}}{\text{m}^2 \text{ sec}}\right)$
-3	visual meteors	20	8×10^{7}	1.4×10^{4}	3.1×10^{-16}
-2	visual meteors	8	3.2×10^{7}	1.4×10^{4}	3.1×10^{-16}
-1	visual meteors	3	1.2×10^{7}	2.2×10^{4}	4.8×10^{-16}
0	visual meteors	1.25	5×10^{6}	3.6×10^{4}	7.9×10^{-16}
1	visual meteors	5×10^{-1}	2×10^{6}	1.1×10^{5}	2.5×10^{-15}
2	visual meteors	2×10^{-1}	8×10^{5}	4.3×10^{5}	9.4×10^{-15}
3	visual meteors	8×10^{-2}	3.2×10^{5}	4.6×10^{5}	1×10^{-14}
4	visual meteors	3×10^{-2}	1.2×10^{5}	3.3×10^{5}	7.2×10^{-15}
3	telescopic meteors	8×10^{-2}	3.2×10^{5}	5.8×10^{5}	1.3×10^{-14}
4	telescopic meteors	3×10^{-2}	1.2×10^{5}	3.0×10^{6}	6.5×10^{-14}
5	telescopic meteors	1.25×10^{-2}	5×10^{4}	2.1×10^{7}	4.6×10^{-13}
6	telescopic meteors	5×10^{-3}	2×10^{4}	9.1×10^{7}	2×10^{-12}
7	telescopic meteors	2×10^{-3}	8×10^{3}	4.3×10^{8}	9.4×10^{-12}
8	telescopic meteors	8×10^{-4}	3.2×10^{3}	5.3×10^{8}	1.2×10^{-11}
9	telescopic meteors	3.1×10^{-4}	1.2×10^{3}	2.0×10^{8}	4.4×10^{-12}

* The momenta are based on mass values from Table I and an average geocentric velocity of 40 Km sec^{-1}.

TABLE XV

VISUAL METEOR DATA

Based on Lovell (51), Pg. 267

Visual Magnitude	Mass (gm) (Lovell)	Median v.m.	Mass (gm) (Table I)	Particle Momentum* $\left(\frac{\text{gm cm}}{\text{sec}}\right)$	No. of Meteors incident on Earth per day	Influx Rate $\left(\frac{\text{particles}}{\text{m}^2 \text{ sec}}\right)$
-10 to - 8	500 gm to 100 gm	- 9	5000	2×10^{10}	300	6.4×10^{-18}
- 7 to - 6	100 gm to 10 gm	- 6.5	500	$\times 10^{9}$	2.5×10^{3}	5.5×10^{-17}
- 5 to - 4	10 gm to 1 gm	- 4.5	80	3.2×10^{8}	1.8×10^{4}	3.9×10^{-16}
- 3 to - 1	1 gm to 100 mgm	- 2	8	3.2×10^{7}	1×10^{5}	2.2×10^{-15}
0 to + 1	100 mgm to 10 mgm	0.5	0.8	3.2×10^{6}	1×10^{6}	2.2×10^{-14}
+ 2 to + 4	10 mgm to 1 mgm	3	8×10^{-2}	3.2×10^{5}	3.6×10^{7}	7.8×10^{-13}
+ 5 to + 6	1 mgm to 0.1 mgm	5.5	8×10^{-3}	3.2×10^{4}	1.9×10^{8}	4.1×10^{-12}
+ 7 to + 9	0.1 mgm to 0.01 mgm	8	8×10^{-4}	3.2×10^{3}	3.3×10^{9}	7.2×10^{-11}
+10 to +12	0.01 mgm to 0.001 mgm	11	5×10^{-5}	2×10^{2}	6.5×10^{10}	1.4×10^{-9}

* The momenta are based on mass values from Table I and an average geocentric velocity of 40 Km sec^{-1}.

Radar Meteor Data

The data tabulated in Table XVI has been derived from data given by Manning and Eshlemann (52).

TABLE XVI

RADAR METEOR DATA

Electron Line Density $\left(\frac{\text{electrons}}{\text{m}}\right)$	Visual Magnitude	Meteor Mass (gm) (Table I)	Particle Momentum* $\left(\frac{\text{gm cm}}{\text{sec}}\right)$	Average Influx Rate $\left(\frac{\text{particles}}{\text{m}^2 \text{ sec}}\right)$
10^{17}	-2.5	12.5	5×10^{7}	1.6×10^{-15}
10^{16}	0	1.25	5×10^{6}	1.6×10^{-14}
10^{15}	2.5	1.25×10^{-1}	5×10^{5}	1.6×10^{-13}
10^{14}	5	1.25×10^{-2}	5×10^{4}	1.6×10^{-12}
10^{13}	7.5	1.25×10^{-3}	5×10^{3}	1.6×10^{-11}
10^{12}	10	1.25×10^{-4}	5×10^{2}	1.6×10^{-10}
10^{11}	12.5	1.25×10^{-5}	5×10^{1}	1.6×10^{-9}
10^{10}	15	1.25×10^{-6}	5×10^{0}	1.6×10^{-8}

* $V_G = 40 \text{ Km sec}^{-1}$

A relationship between the visual magnitude and the mass of a radar meteor was not specified by Manning and Eshlemann, so the relationship shown by the data of Table I was applied in order to convert the data given by Manning and Eshlemann into a form usable in the composite analysis.

CHAPTER IX

A COMPOSITE ANALYSIS

The data from Chapter VII and Chapter VIII may be combined to yield a composite set of meteoric influx data. The composite set of data consists of the following subsets:

1. Data from rockets and satellites in the United States.
2. Data from the Soviet Union's Sputnik I. (38).
3. Influx estimates based on observations of zodiacal light by:
   (a) Beard (49)
   (b) Seidentopf (18)
   (c) Takakubo (16).
4. Representative data for visual meteors given by:
   (a) Watson (1)
   (b) Watson (50)
   (c) Lovell (51).
5. Radar meteor data given by Manning and Eshlemann (52).

The composite set of data encompasses a considerable range of mass for meteoric particles. The influx rates measured on the rockets, together with the estimates based on the observations of zodiacal light, should represent sufficient justification for making a tentative revision of the mass distribution function. The composite set of data is shown in graphical form in Figure 12.

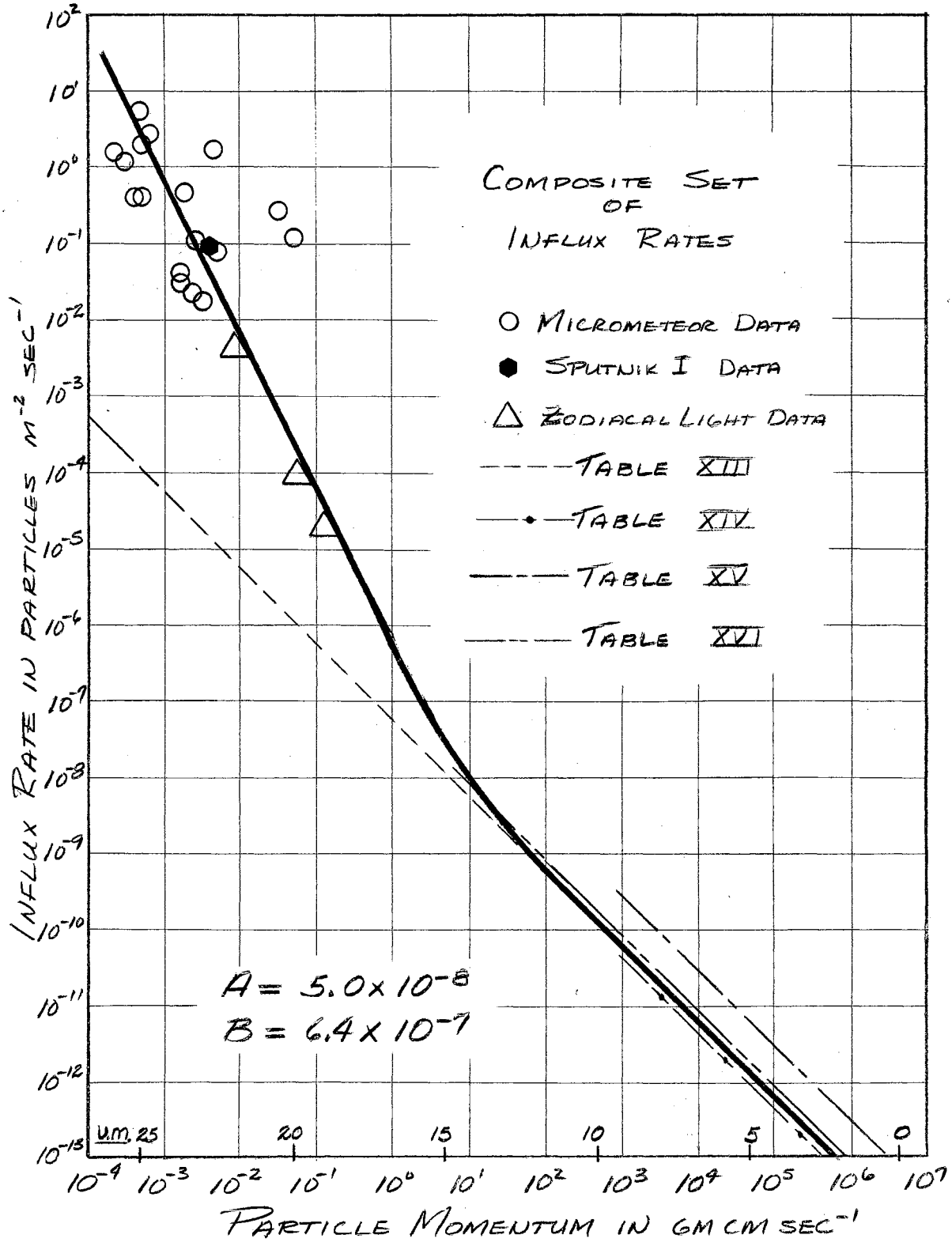

Figure 12. A Plot of the Composite Set of Influx Rates.

Figure 12 is actually a plot of meteoric influx rate as a function of particle momentum. (Visual magnitude numbers are inserted along the abscissa to facilitate references to the figure). An average geocentric velocity has been used throughout the analysis, so the abscissa in Figure 12 could be changed to particle mass by simply dividing all the momenta by the average geocentric velocity. Such a procedure would yield the mass distribution function which is the item of primary interest. Micrometeors are, however, described most conveniently in terms of their momenta, so the question of whether to use particle mass or particle momentum as the abscissa arises. The use of momentum as the independent variable proves to be the most convenient, because all the micrometeor data has been given in terms of the particle momentum. Therefore, we retain influx rate and momentum as the ordinate and abscissa, respectively, in Figure 12, and at the same time speak of the mass distribution function in conjunction with Figure 12.

Application of the method of least squares to the micrometeor influx data shown in Table XI has led to values of p (p is the magnitude of the slope of the mass distribution curve on a log-log plot) from 0.4 to 1.4. The various values for p were obtained through the use of various schemes of weighting for the micrometeor influx datum points. None of the values of p obtained through the use of the method of least squares allowed a straight line segment of the mass distribution curve to pass through the micrometeor datum points, and at the same time, to join smoothly onto the constant mass per unit visual magnitude curve either in or slightly above the faint radar meteor range of mass values. One of the most successful trials with the method of least squares gave $p = 1.4$ and $B = 2.2 \times 10^{-5}$. Therefore, an alternate method of

determining the upper portion of the curve was employed. A discussion of some of the possible implications of the failure of the method of least squares to give a satisfactory curve will be presented later.

The lower portion of the mass distribution curve of Figure 12 may be represented by a straight line segment. Let us assume that the upper portion of the curve may also be represented approximately by a straight line segment, and that the upper and lower portions of the curve join smoothly somewhere above the radar meteor range. The heavy solid curve in Figure 12 is of the type just described.

The lower portion of the curve in Figure 12 may be slightly in error, since the mass to visual magnitude relationship defined by Table I has been used in determining the masses for the visual and radar meteors. The choice of smaller mass values for visual and radar meteors would shift the lower portion of the curve slightly to the left. The basic form of the curve remains unchanged even though the lower portion of the curve is shifted parallel to itself by a slight amount.

Since the curve of Figure 12 is on a log-log plot, and the upper and lower portions of the curve both appear to be straight lines, the equation of the composite curve may be taken as the sum of the equations of the upper and lower portions of the curve. The equation of the upper portion of the curve makes a negligible contribution to the composite curve for momenta values higher than about 10^2 gm cm sec^{-1}, and the equation of the lower portion of the curve makes a negligible contribution to the composite curve for momenta values lower than about 1 gm cm sec^{-1}. The problem has now reduced to finding the equations of the upper and lower portions of the composite curve and of evaluating the constants appearing in the equations.

The equation of the lower portion of the curve in Figure 12 is of the form

$$I = \frac{A}{M}, \tag{1}$$

where A is a constant associated with a particular set of observations, and M is the momentum of a meteor or micrometeor. A change of A moves the lower portion of the curve parallel to itself without affecting the slope of the curve. Various values of the constant A may be determined for different sets of visual meteor data chosen to represent the lower portion of the mass distribution curve. The equation (1) implies a constant mass per unit visual magnitude relationship--an extension of the curve out to a visual magnitude of +30 is the type of extrapolation performed by Watson in order to get the constant mass per unit visual magnitude relationship as a mass distribution function.

The equation of the upper portion of the curve shown in Figure 12 appears to be of the form

$$I = \frac{B}{M^p}, \tag{2}$$

where B is a constant, and p is the negative of the slope of the upper portion of the curve. A line corresponding to p = 2 seems to fit the micrometeor data fairly well, and at the same time, to join onto the lower section of the curve just above the radar meteor range. The micrometeor influx rates shown in Figure 12 represent about the lowest that can be obtained through a reasonable analysis of the existing flight data and should serve as somewhat of a lower bound on the influx rates of the micrometeors.

The equations for the two separate portions of the composite mass distribution curve may now be combined to yield an equation of the form

$$I = \frac{A}{M} + \frac{B}{M^2}. \tag{3}$$

The alternate method of determining the mass distribution function consists of re-plotting Figure 12 onto a very large sheet of log-log graph paper. Remembering which of the micrometeor datum points are probably the most reliable, we fit the upper portion of the curve (of slope -2) to the micrometeor datum points by visual inspection. Once the curve is positioned, the value of B may be determined for use in equation (3). If the data of Table XIII is accepted as fairly representative of all visual meteor data, then a correspondingly representative value of the constant A may also be determined. An equation that seems to fit the curve of Figure 12 fairly well is

$$I = \frac{5 \times 10^{-8}}{M} + \frac{6.4 \times 10^{-7}}{M^2}, \qquad (4)$$

where A has been based on the data of Table XIII, and B has been determined by visual inspection of the enlarged version of Figure 12.

One might, upon looking at the zodiacal light datum points of Figure 12, be tempted to choose a value of p less than 2 in order to decrease the slope of the upper portion of the curve until the upper portion of the curve fitted the zodiacal light datum points better. However, before making such a choice, one should remember the method used (see Chapter VIII) to get the zodiacal light datum points. The micrometeor datum points are probably far more reliable than the zodiacal light datum points. Hence, any shift in the upper portion of the composite curve should favor the micrometeor datum points.

If the equation (4) is considered to represent, satisfactorily, the photographic, visual, and radar meteor data, the influx rates predicted from observations of zodiacal light and solar F corona, and the recent measurements of the influx rates of micrometeors, then the next question to arise should logically be concerned with the range of momentum over

which the equation (4) is valid. The new mass distribution function fits the micrometeor data out to a momentum of about 2×10^{-4} gm cm sec^{-1} (26 v.m.) quite well.

The radiation pressure effect is quite effective for particles with radii smaller than about 1μ. A particle of radius 1μ corresponds to a particle with a momentum of about 5×10^{-6} gm cm sec^{-1} or a visual magnitude of about +30. Therefore, the validity of extending the new mass distribution function out to +30 v.m. is quite questionable, especially since we have encountered difficulty in applying the method of least squares to the micrometeor influx data. Since the extension may be questionable, let us extrapolate the micrometeor data out to only about +26 v.m. Then the mass distribution function and its range of validity will appear something as follows:

$$I = \frac{A}{M} + \frac{B}{M^2}, \qquad (5)$$

where the constants are $A = 5 \times 10^{-8}$, $B = 6.4 \times 10^{-7}$, and the range of momentum is

$$(5 \times 10^{8} \text{ gm cm sec}^{-1}) > M \geq (2 \times 10^{-4} \text{ gm cm sec}^{-1}),$$

which corresponds to a range of visual magnitude of -5 to +26.

Now, let us return to the question of getting the curve, obtained through the method of least squares for the micrometeor influx datum points, to join onto the constant mass per unit visual magnitude curve at a point above the radar meteor range. The upper portion of the curve must not join the lower portion below the radar meteor range, because no appreciable deviations from the constant mass per unit visual magnitude curve have been reported for meteors up to and including the radar meteors. However, none of the values of p determined through use of the

method of least squares provides a curve that joins onto the lower portion of the curve at a point above the radar meteor range. In fact, p = 1.4 corresponds to a junction of the curves at about 5 v.m.

In order to investigate the validity of our choice of a single straight line segment as the upper portion of the distribution curve, we should try to determine how we expect the mass distribution curve to behave in the neighborhood of +30 v.m. Meteoric particles with visual magnitudes greater than about +30 v.m. are removed from the solar system by the effect of radiation pressure. Thus, if there is no source for producing particles of visual magnitude greater than +30 within 1 A.U. of the Sun, there should be no such particles at the Earth's orbit, and hence the influx rate would drop to zero for visual magnitudes greater than +30. This means that the mass distribution curve is going to have to show a marked change between +25 v.m. and +30 v.m. If the micrometeor datum points just happen to be falling on the "knee" of the mass distribution curve, the slopes given by the method of least squares may begin to have some meaning. This possibility is shown in a qualitative manner in Figure 13.

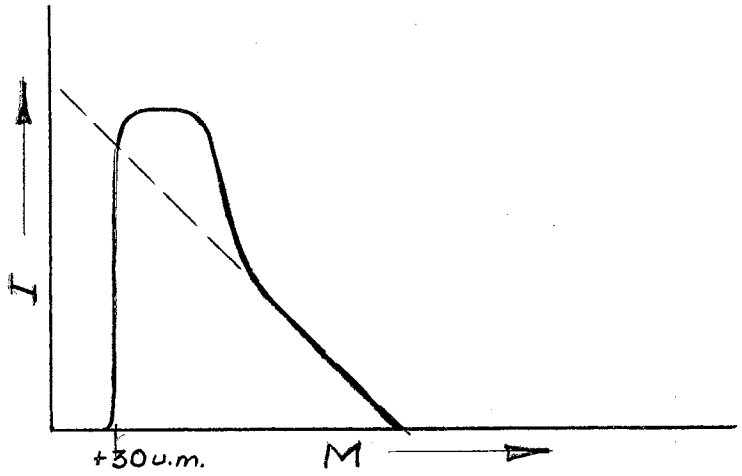

Figure 13. A Mass Distribution Curve with a Radiation Pressure Cut-off.

The curve shown in Figure 13 corresponds to the complete absence of a source of meteoric particles of visual magnitude greater than about +30 within 1 A.U. of the Sun. An inspection of Figure 12 reveals that the upper portion of the curve need not have an initial slope of greater than -2 in order to behave as shown in Figure 13. Also, the datum points of momentum sensitivity scales S_2 and S_3 on the diaphragm of Aerobee #80 and S_3 on Cajun AA6.202 may begin to have more meaning if a curve of the type shown if Figure 13 is considered. These datum points appear to be lying on a higher-than-normal mass distribution curve on the range +17.5 to +25 v.m.

The presence or non-presence of a source of particles of greater than +30 v.m. inside the orbit of Earth may affect, quite markedly, the shape of the mass distribution curve. For example, if there were an especially prolific source of such particles within 1 A.U. of the Sun, the mass distribution curve might conceivably continue to rise for visual magnitudes greater than +30 in a manner similar to that shown in Figure 14.

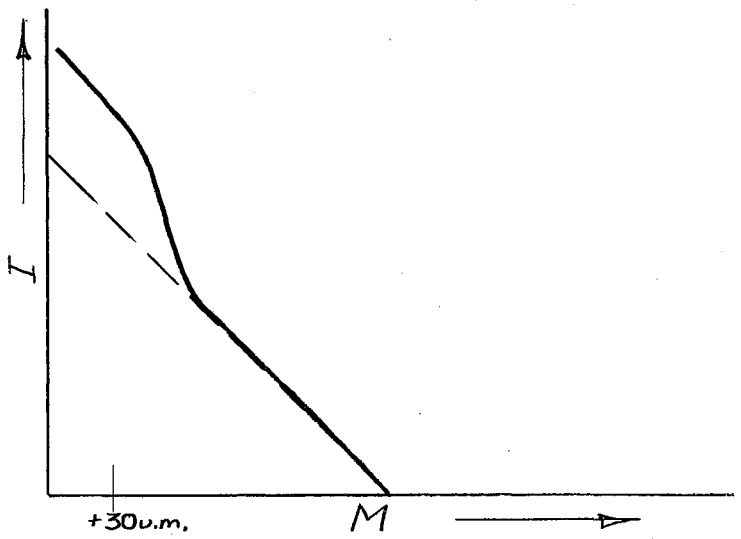

Figure 14. Possible Form of the Mass Distribution Curve if a Large Source of Extremely Small Micrometeors Exists within 1 A.U. of the Sun.

If the source of meteoric particles smaller than +30 v.m. is weaker than the source represented in Figure 14, the mass distribution curve might appear more like the curve shown in Figure 15.

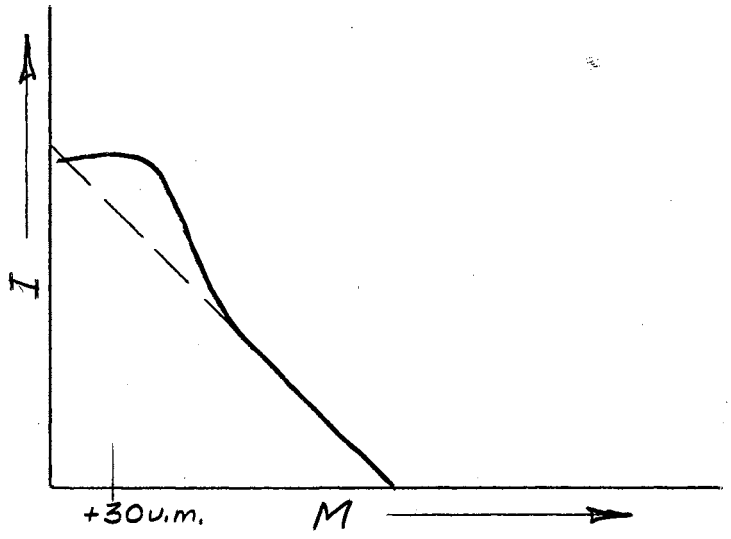

Figure 15. Possible Form of the Mass Distribution Curve if a Moderate Source of Extremely Small Micrometeors is Present.

There is an acute need for experimental data over a considerably larger range of momentum than the data that is now available. Data for meteoric particles with masses between those of radar meteors and micrometeors and data for particles with visual magnitudes in the neighborhood of +30 would help considerably in determining the trend of the mass distribution curve in those regions of visual magnitude. More quantitative influx data is needed before much can be done towards finding the specific shape of the mass distribution curve on the range of +15 to +30 v.m.

CHAPTER X

RESULTS OF THE INVESTIGATION

The measurements of micrometeoric influx rates made recently on a series of high-altitude rockets and an Earth satellite exceed, by several orders of magnitude, the influx rates predicted by the presently accepted mass distribution function. The measurements are quite consistent with one another, and no reasonable methods of analysis cause the influx rates to change appreciably.

The measured micrometeor influxes have been used to find a new mass distribution function of the form

$$I = \frac{A}{M} + \frac{B}{M^2}$$

to tentatively replace the presently accepted mass distribution function of the form

$$I = \frac{A}{M} .$$

When the equation

$$I = \frac{A}{M} + \frac{B}{M^2}$$

is fitted to the experimental datum points by a visual inspection technique, we find that

$$A \doteq 5 \times 10^{-8}$$
$$B \doteq 6.4 \times 10^{-7} .$$

According to this new mass distribution function, the influx rate for +25 v.m. micrometeors is 2.5×10^4 higher than the rate predicted by the constant mass per unit visual magnitude relationship.

The new mass distribution function differs appreciably from the old mass distribution function for meteoric masses smaller than the radar meteors. The new mass distribution function appears to resolve some of the difficulties encountered during the past decade by investigators who have tried to predict the rate of influx of meteoric material on the basis of observations of zodiacal light and solar F corona.

The new mass distribution function is valid for meteoric particles up to at least +25 v.m., and possibly up to about +26 v.m. Extension of the function past +30 v.m. would be of very doubtful validity until more experimental investigations have been made to see how the mass distribution function behaves in the neighborhood of the radiation pressure limit at about +30 v.m.

CHAPTER XI

IMPLICATIONS OF THE ANALYSIS AND SUGGESTIONS FOR FUTURE INVESTIGATION

Probably the most important implication provided by the new mass distribution function is that the rate of accretion of meteoric material by Earth is much higher than previously expected. Higher influx rates imply, in turn, higher energy inputs to the upper atmosphere of Earth. Also important is the fact that the major portion of the accreted mass, according to the new mass distribution function, is supplied by the very small micrometeors.

In the past, the contributions to the sporadic E layer of Earth's ionosphere by the influx of meteors have been considered negligible because no correlation between sporadic E and the meteor showers could be found. The meteor showers are probably deficient in micrometeors, with the largest particles producing effects at altitudes below that of the E layer. The consideration of deceleration of the micrometeors by the atmosphere shows that the region of maximum deceleration for micrometeors of, say +25 v.m., and the E region are practically coincident. It seems plausible, therefore, that the high micrometeor influx rates may possibly be associated with at least some component of the sporadic E. The energy supplied to the atmosphere by the incident meteoric particles increases during the night as the side of the Earth on which the observer is stationed turns into a position such that the particles are met

head-on. The higher-than-expected micrometeor influx rates may have at least some connection with the night-time sources of ionization in the E region.

Another interesting aspect of the mass distribution function is the behavior of the function in the neighborhood of +30 v.m. Meteoric particles of less than 1 μ radius should have already been removed from the inner part of the solar system unless some means for producing micrometeors exists within 1 A.U. of the Sun. Could the particles of cometary origin be partially evaporated by the Sun only to be blown back out past the orbit of Earth by radiation pressure? To what extent does the Earth gather a "space cloud", as proposed by Beard (49), of the small micrometeors as Earth moves along its orbit? How far out from the Earth does the "space cloud" extend? Could the accumulation of interstellar matter by the solar system as it moves through space be responsible for the supply of small micrometeors? Is there a "grinding" process going on among the smaller particles of the asteroid belt of sufficient activity to maintain the higher influx of micrometeors?

If the micrometeors were found to be predominantly of iron type rather than of stony type (the stony type is implied by a cometary origin), what would be the cosmogonal importance of such a result? Does the cloud of micrometeoric dust in the solar system have spherical symmetry about the Sun as might be implied by the increasing randomness of orbit orientations found as fainter visual and radar meteors were observed?

When do the effects of the micrometeors on the atmosphere of Earth become important because of the photoelectric charge that has surely been induced through long exposures of a micrometeor in intense cosmic

radiation? What types of ionospheric effects will occur if the micrometeors "stack up" in the E region or at altitudes somewhat lower than the E region?

A majority of the questions posed in the preceding paragraphs have an importance regardless of the form of the mass distribution function. However, some of the questions assume an even greater importance if the new mass distribution function proves to be valid.

Specific topics that should be considered in the near future are the possibility of getting satellite vehicles equipped with micrometeor detection equipment so longer data sampling times can be obtained, the development of new means of detecting the particles of micrometeoric size so the acoustical type of micrometeor detection system can be both double-checked and supplemented, and the determination of the approximate shape of the distribution curve at about +30 v.m. so detection equipment can be designed accordingly. Also, satellite vehicles of fairly large surface area could be used to obtain data on the meteoric masses intermediate to radar meteors and micrometeors.

A SELECTED BIBLIOGRAPHY

1. Watson, Fletcher G., Between the Planets, Harvard University Press, Cambridge (1952).

2. Hey, J. S., and G. S. Stewart, "Derivation of Meteor Stream Radiants by Radio Reflexion Methods", Nature, 158 481 (1946).

3. Opik, Ernst J., Physics of Meteor Flight in the Atmosphere, Interscience Publishers, Inc., New York (1958).

4. Opik, Ernst J., (Title unknown), Tartu Obs. Publ., 25 (1) (1922).

5. Lindemann, F. A., and G. M. B. Dobson, "Theory of Meteors and Density and Temperature of the Outer Atmosphere to Which It Leads", Proc. Roy. Soc., London, 411 102 (1923).

6. Sparrow, C. M., "Theory of Meteors", Ap. J., 63 90 (1926).

7. Lindemann, F. A., "A Note on Theory of Meteors", Ap. J., 65 117 (1927).

8. Maris, H. B., "A Theory of Meteors", Terr. Mag. and Atm. Elec., 34 (4) 309 (1929).

9. Opik, Ernst J., "Basis of the Physical Theory of Meteor Phenomena", Tartu Obs. Publ., 29 (5) (1937).

10. Herlofson, N., "The Theory of Meteor Ionization", Rep. Phys. Soc. Prog. Phys., 11 444 (1948).

11. Grimminger, G., "Probability that a Meteorite Will Hit or Penetrate a Body Situated in the Vicinity of Earth", J. App. Phys., 19 (10) 947 (1948).

12. Rocket Panel, The, "Pressures, Densities, and Temperatures in the Upper Atmosphere", Phys. Rev., 88 (5) 1027 (1952).

13. Horowitz, R., and H. E. LaGow, "Upper Air Pressure and Density Measurements from 90 to 220 Km with the Viking 7 Rocket", J. Geophys. Res., 62 (1) 57 (1957).

14. Horowitz, R., and H. E. LaGow, "Summer-Day Auroral-Zone Atmospheric-Structure Measurements from 100 to 210 Kilometers", J. Geophys. Res., 63 (4) 757 (1958).

15. van de Hulst, H. C., "Zodiacal Light in the Solar Corona", Ap. J., 104 471 (1947).

16. Takakubo, K., "Continuous Light of the Solar Corona", P.A.S. Japan, 2 14 (1950).

17. Whipple, F. L., "Origin of the Zodiacal Cloud", In Meteors, Permagon Press Ltd., London (1955), Pg. 144.

18. Siedentopf, H., "Diffuse Matter in the Solar System", In Meteors, Permagon Press Ltd., London (1955), Pg. 145.

19. Dubin, Maurice, "Meteoric Bombardment", In Scientific Uses of Earth Satellites", The University of Michigan Press, Ann Arbor (1956), Pg. 292.

20. Whipple, Fred L., "The Theory of Micrometeors", Proc. Nat'l. Acad. Sci., 36 687 (1950); 37 19 (1951).

21. Cook, M. A., H. Eyring, and R. N. Thomas, "The Physical Theory of Meteors, Part I. A Reaction-Rate Approach to the Rate of Mass Loss in Meteors", Ap. J., 113 475 (1951).

22. Thomas, Richard N., and Fred L. Whipple, "The Physical Theory of Meteors, Part II. Astroballistic Heat Transfer", Ap. J., 114 448 (1951).

23. Thomas, Richard N., "The Physical Theory of Meteors, Part III. Conditions at the Meteor Surface", Ap. J., 116 203 (1952).

24. Thomas, Richard N., and William C. White, "The Physical Theory of Meteors, Part IV. Inquiry into the Radiation Problem--A Laboratory Model", Ap. J., 118 555 (1953).

25. Smith, Henry J., "The Physical Theory of Meteors, Part V. The Masses of Meteor Flare Fragments", Ap. J., 119 438 (1954).

26. Cook, Allan F., "The Physical Theory of Meteors, Part VI. The Light Curve", Ap. J., 120 572 (1954).

27. Whipple, Fred L., "The Physical Theory of Meteors, Part VII. On Meteor Luminosity and Ionization", Ap. J., 121 241 (1955).

28. Jacchia, Luigi G., "The Physical Theory of Meteors, Part VIII. Fragmentation as Cause of the Faint Meteor Anomaly", Ap. J., 121 521 (1955).

29. Dubin, Maurice, "Interplanetary Matter and the Earth Satellite", (A paper presented at the VII International Astronautical Congress, Rome, Italy, 17-22 September 1956).

30. Dubin, Maurice, "Meteor Impacts by Acoustical Techniques", In Rocket Exploration of the Upper Atmosphere, Interscience Publishers, Inc., New York (1954), Pg. 26.

31. Dubin, Maurice, "Meteoric Ionization in the E Region", In Meteors, Permagon Press Ltd., London (1955), Pg. 111.

32. Dubin, Maurice, "Cosmic Debris of Interplanetary Space", (A paper presented at the Second OSR Astronautics Conference at Denver, Colorado, 28 April 1958).

33. Dubin, Maurice, "Direct Measurements of Meteoritic Dust Using Rockets and Satellites", (A paper presented at the Tenth General Assembly of the Astronomical Union, Moscow, USSR, August 1958).

34. Manring, Edward R., "Micrometeorite Measurements from 1958α and γ Satellites", Plan. and Sp. Sci., 1 (1) 27 (1959).

35. Kaiser, T. R., (editor), Meteors, Special Supplement (Vol II) to the Journal of Atmospheric and Terrestrial Physics, Permagon Press Ltd., London (1955).

36. Berg, O. E., and L. H. Meredith, "Meteorite Impacts to Altitudes of 103 Kilometers", J. Geophys. Res., 61 751 (1956).

37. Bauer, Carl A., "Interpretation of Responses of a Meteorite Detector on a Rocket", (Abstract of a paper given at the 100th meeting of the AAS), A. J., 63 (1262) 302 (1958).

38. Nazarova, I. N., "Rocket and Satellite Investigation of Methods--Study of Meteors on Rockets and Satellites", (A paper presented at the 5th meeting of IGY Special Committee at IAU meeting, Moscow, USSR, August 1958).

39. Whipple, Fred L., "On Meteor Masses and Densities", (Abstract of a paper given at the 86th meeting of the AAS), A. J., 57 (1197) 28 (1952).

40. Wyatt, Stanley P., and Fred L. Whipple, "The Poynting-Robertson Effect on Meteor Orbits", Ap. J., 111 134 (1950).

41. Allen, C. W., Astrophysical Quantities, The Athone Press, University of London (1955).

42. McKinley, D. W. R., "Meteor Velocities Determined by Radio Observations", Ap. J., 113 225 (1951).

43. Yagoda, H., "Electrographic and Contact Printing Methods for the Study of Cosmic Dust Impacts on Mesospheric Vehicles", Proc. High Speed Impact Symposium, Rand Corporation, Santa Monica, California (1955).

44. Yagoda, H., "Micro-Meteorite Observations from the Flight of USAF Aerobee 77", (An unpublished paper).

45. Staff, Oklahoma State University Research Foundation Electronics Laboratory, Quarterly Status Reports Nos. 1 to 11 on Contract No. 19(604)-1908.

46. Zwicky, F., "The Possibility of Earth Launched Meteors", P.A.S. Pacific, 58 260 (1946).

47. Halliday, David, Introductory Nuclear Physics, John Wiley & Sons, Inc., New York (1955).

48. McCracken, Curtis W., and G. R. Huggett, "Calibration of a Rocket-Borne Micrometeorite Detection System", (An unpublished term paper written at Oklahoma State University, 5 April 1957).

49. Beard, David B., "Interplanetary Dust Distribution", Ap. J., 129 (2) 496 (1959).

50. Watson, Fletcher G., "Distribution of Meteoric Masses in Interstellar Space", Harv. Ann., 105 (1937), Pg. 623.

51. Bates, D. R., (editor), The Earth and its Atmosphere, Basic Books, Inc., New York (1957).

52. Manning, L. A., and V. R. Eshleman, "Meteors in the Ionosphere", Proc. IRE, 47 (2) 186 (1959).

APPENDIX A

MASS TO VISUAL MAGNITUDE RELATIONSHIPS FOR METEORS

The kinetic energy of a meteoric mass incident on Earth's upper atmosphere is converted into heat, light, and ionization. The portion of the kinetic energy which appears as visible light is given by

$$I t = \tau \frac{1}{2} m_o v_6^2 \qquad \text{(a-1)}$$

where: I is the luminous intensity,

t is the time required for the luminous meteor trail to form,

τ is the luminous efficiency,

m_o is the original mass of the meteor, and

v_6 is the original geocentric velocity of the meteor.

Solving equation (a-1) for m_o, we have

$$m_o = \frac{2 I t}{\tau v_6^2} \qquad \text{(a-2)}$$

Apparent visual magnitude (v.m.) is defined in terms of the luminous intensity through the relationship

$$\log I = 9.72 - 0.4 \text{ v.m.} \qquad \text{(a-3)}$$

in which the term 9.72 is based on the assignment of a visual magnitude of -26.72 to Sun. (3).

Next, we take the logarithm of equation (a-2) to get

$$\log m_o = \log 2 + \log I + \log t - \log \tau - 2 \log v_6 . \qquad \text{(a-4)}$$

Substitution of equation (a-3) into equation (a-4) gives

$$\log m_o = \log 2 + 9.72 - 0.4 \text{ v.m.} + \log t - \log \tau - 2 \log v_6 . \qquad \text{(a-5)}$$

Opik (3) gives, for his Arizona meteor expedition,

$$t = 0.67 \left(\frac{2.1 \times 10^6}{v_6}\right)^{0.7}$$

which becomes, upon letting v_6 be 40 kilometers per second,

$$t = 0.417 \text{ SEC.}$$

Substituting the numerical values of v_6 and t into equation (a-5) and collecting terms, we get

$$\log m_0 = -3.563 - \log \tau - 0.4\, v.m. \qquad \text{(a-6)}$$

which is an expression for the mass of a meteor as a function of the luminous efficiency and the visual magnitude. Once the luminous efficiency is specified, equation (a-6) will serve to relate mass and visual magnitude. According to Opik (3), $\tau < 0.003$. If $\tau = 0.003$, then

$$\log m_0 = -0.563 - 0.4\, v.m., \qquad \text{(a-7)}$$

and a 0 v.m. meteor will have a mass of 0.275 gm. This value of the mass is larger than the value given in either Table XIII or Table XV. The use of a value of τ less than 0.003 leads to even larger values of mass for a given visual magnitude meteor than were obtained through the use of equation (a-7).

Next, we wish to calculate the value of τ that will go with the mass values given in Table I. Using equation (a-6) for a 0 v.m. meteor, we get

$$\log \tau = -3.563 - \log m_0. \qquad \text{(a-8)}$$

A 0 v.m. meteor has a mass, according to Table I, of 1.25 gm, so

$$\tau \doteq 2.2 \times 10^{-4}.$$

Although the value, 0.00022, for τ is more than an order of magnitude smaller than the upper limit given by Opik for τ, the value does not seem unreasonable.

An equation similar to equation (a-7) may be obtained from the data

of Table I. The equation is

$$\log m_0 = 0.09691 - 0.4\, v.m. \qquad \text{(a-9)}$$

Therefore, until the luminous efficiency has been determined sufficiently accurate to allow the visual and radar meteor investigators to specify the masses of such meteors to within an accuracy much greater than an order of magnitude, we may use an arbitrary scale such as that of Table I in our various computations.

APPENDIX B

A CONSIDERATION OF EFFECTIVE AREA

The effective area of a micrometeor detecting surface is a quantity needed in the determination of the influx rate for a given set of micrometeor observations. The effective area is used, along with the total number of micrometeoric impacts and the data sampling time, in the computation of the influx rate of the micrometeoric particles. The use of the total surface area of the detecting surface as the effective area does not seem to be the most reasonable choice because of two major reasons. These reasons are that sections of a micrometeor detecting surface may, at times, lie shielded by Earth from receiving any micrometeoric impacts and that the flux pattern for the micrometeors is probably more complicated than a radial flux isotropic over 4π steradians. The cases treated in the following paragraphs are for the simplest flux patterns and shapes of micrometeor detecting surfaces.

One of the simplest cases is that shown in Figure 16, in which a cylindrical micrometeor detecting surface is placed with its axis

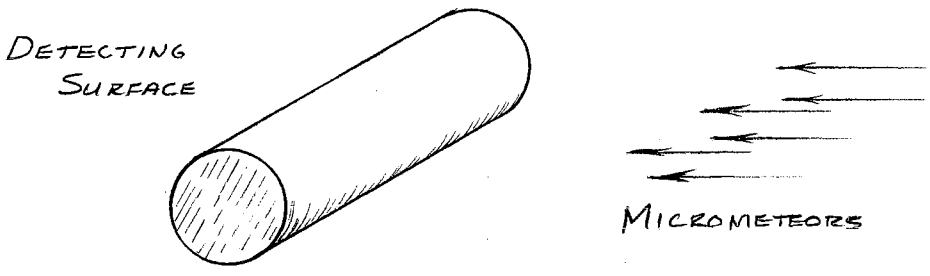

Figure 16. Diagram of a Cylindrical Detecting Surface Placed in a Collimated Beam of Micrometeors.

perpendicular to the direction of motion of a collimated beam of micrometeors. Assume that the microphone attached to the detecting surface is sensitive to only the normal component of the impulse delivered to the detecting surface by an incident micrometeor. Figure 17 is a cross-sectional view of the cylinder showing various angles of incidence for the micrometeoric particles.

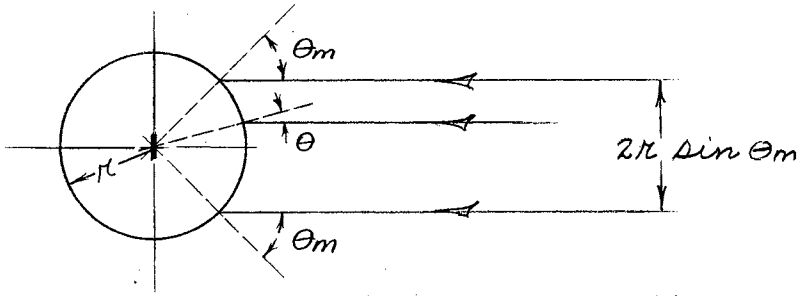

Figure 17. Diagram Showing Various Angles of Incidence for the Micrometeors of a Parallel Beam.

The normal component of the impulse delivered by a particle incident at an angle θ with respect to the unit normal $\vec{n}$ to the surface at the point of impact is

$$M_n = m\vec{v}\cdot\vec{n} = mv\cos\theta \qquad \text{(b-1)}$$

where m is the mass and v is the velocity of the micrometeor. Not all of the particles incident on the surface produce measurable impulses because of the variation with θ of the normal component of the impulse. A maximum, θ_m, of the values of θ that produce measurable impulses may be chosen on the basis of the type of collision involved. A maximum angle of incidence, $\theta_m = 60°$, allows a variation in the detectable impulse of a factor of 2. A variation of a factor of 2 is probably acceptable in most considerations. However, a simplification is possible in a later section if $\theta_m = 45°$ is chosen.

The section of surface shown in Figure 17 may be replaced by a plane surface of which the normal makes an angle of θ_m with the

direction of motion of the incident micrometeors. The equivalent surface is shown in Figure 18.

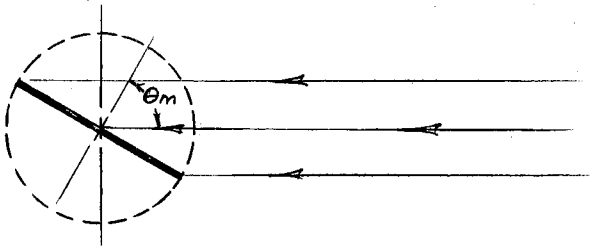

Figure 18. The Equivalent Detecting Surface.

The surface shown in Figure 18 is called the equivalent surface, because of its ability to detect all the particles with $\theta \leq \theta_m$ that could have been detected on the section of the cylindrical surface. The equivalent surface has an area, for a cylinder of radius r and length l, of $2rl$, which is just the area of an axial cross-section of the cylinder.

The effective area of the equivalent surface for the collimated beam flux pattern is

$$A_E' = 2rl \sin\theta_m \qquad \text{(b-2)}$$

The equivalent surface shown in Figure 18 has an additional feature in that the surface is capable of detecting also particles coming from directions other than that of the collimated beam. Figure 19 may serve to illustrate the flux pattern to which the equivalent surface is sensitive.

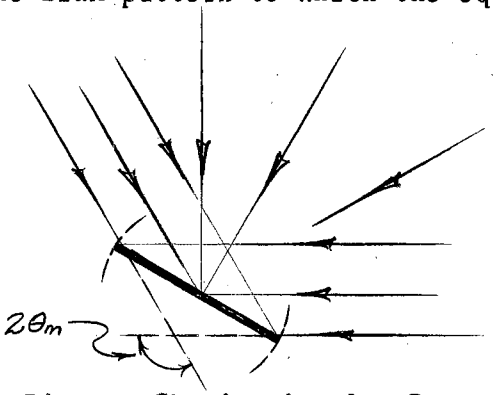

Figure 19. Diagram Showing Angular Responsiveness for the Equivalent Detecting Surface.

The angular spread of directions from which the particles may come in order to produce detectable impulses is just $2\theta_m$. For the case of $\theta_m = 45^\circ$, the angular spread is 90°. The value of 90° suggests the possibility of placing two equivalent surfaces together, as shown in Figure 20, in order to obtain an equivalent surface capable of detecting particles from any direction within 180°.

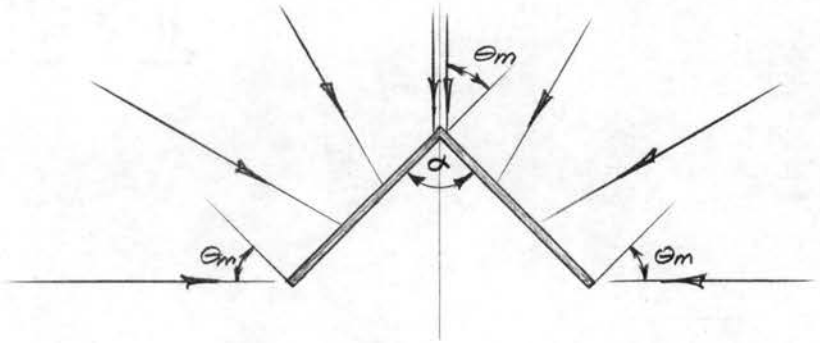

Figure 20. Combination of Equivalent Surfaces.

The angle α between the two equivalent surfaces is 90° when $\theta_m = 45^\circ$. The effective area (as far as θ is involved) of the equivalent surface shown in Figure 20 is just

$$A_E^\theta = 2(2rl)$$
$$A_E^\theta = 4rl = 2A_A$$
$$A_E^\theta = \frac{2}{\pi} A$$

where A_A is the area of an axial cross-section of the cylinder, and A is the total surface area of the cylinder.

The next step towards defining an effective area for the cylinder is letting particles be incident on the cylinder at angles other than 90° with respect to the axis of the cylinder. An axial cross-section of the cylinder, with the θ_m condition applied, is shown in Figure 21. The responsiveness of the cylindrical detecting surface is limited to an angle of $2\theta_m$ for the configuration illustrated in Figure 21. For most

vehicles, the ends of the cylindrical section are left open or are not made sensitive to micrometeoric impacts.

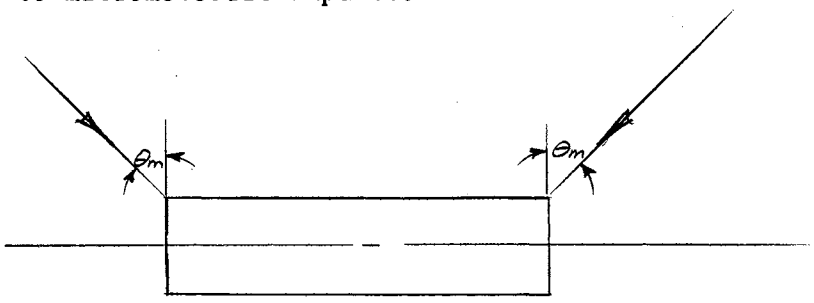

Figure 21. Axial Cross-section of the Cylindrical Detecting Surface, Showing Maximum Angles of Incidence.

Taking into account the angular responsiveness illustrated in Figures 20 and 21, we may define the approximate effective area for the cylinder placed in an isotropic flux of particles (limited to 2π steradians by the shielding effect of Earth) as

$$A_E \doteq \frac{2\theta_m}{180^\circ} \frac{4\theta_m}{180^\circ} 2A_A \qquad \text{(b-4)}$$

which becomes, for $\theta_m = 45^\circ$,

$$A_E \doteq A_A$$

$$A_E \doteq \frac{A}{\pi} . \qquad \text{(b-5)}$$

The total surface area of an Aerobee rocket is about 1.2 m^2. The effective area of the Aerobee rocket, as given by equation (b-5), is 0.38 m^2. Similarly, for a Cajun rocket of surface area 0.43 m^2, the effective area is 0.14 m^2. In comparison, Dubin specifies 0.5 m^2 and 0.2 m^2 as the effective areas for the Aerobee and Cajun, respectively. The effective areas calculated through the use of equation (b-5) are at least comparable to the values specified by Dubin.

Taking the effective areas given by Dubin and equation (b-4), we may solve for the appropriate values of θ_m. The values of θ_m so obtained are 50° and 54° for the Aerobee and Cajun, respectively. Thus, the effective areas specified by Dubin (and used in the analysis in this

paper) are probably about the most representative values available at the present time. A better knowledge of the nature of the collision of a hypervelocity particle onto a detecting surface will allow a better determination of the maximum angle of incidence. In turn, better geometrical representations, to be used in the determination of the equivalent surfaces, can be constructed.

The author did not, in making the analysis presented in this paper, have access to information on the details of the method employed by Dubin in determining the effective areas of the Aerobee and Cajun rockets. Therefore, an attempt to justify the values given by Dubin has been made in the preceding paragraphs, and the effective areas given by Dubin have been used in the computation of the influx rates for the various sets of micrometeor data.

Orientations of the cylinder (or more complicated shapes of detecting surfaces) other than the orientations illustrated in Figure 16 or represented in Figure 19 may be considered. However, most of the other conceivable flux patterns seem to be more difficult to analyze than the ones considered.

APPENDIX C

A CONSIDERATION OF CALIBRATION BEAD VELOCITIES

Consider a small, spherical glass bead that is falling in a viscous fluid. If the instantaneous velocity of the bead is small in comparison to the speed of sound in the fluid, the use of a viscous force that is proportional to the first power of the velocity of the bead will lead to fairly accurate results for the motion of the bead. This viscous force is the same as the viscous force given by Stoke's law for particles moving at their terminal velocities. The viscous force acting on the bead, as given by Stoke's law, is

$$f = 6\pi\eta a v$$

where: η is the coefficient of viscosity for the fluid,

a is the radius of the bead, and

v is the velocity of the bead.

Newton's second law becomes, for the spherical glass bead falling in a viscous fluid,

$$\Sigma F = m\frac{dv}{dt}$$

$$\Sigma F = w - B - f$$

where: w is the weight of the bead,

B is the buoyant force acting on the bead,

f is the viscous force acting on the bead, and

m is the mass of the bead.

The buoyant force is given by

$$B = \frac{4}{3}\pi a^3 \rho g$$

where ρ is the density of the fluid.

For the case of glass beads of density, ρ_G, falling through the atmosphere of Earth near lea level,

$$\rho_G \doteq 2.2 \text{ gm cm}^{-3}, \quad \rho = 1.29 \times 10^{-3} \text{ gm cm}^{-3}$$

$$\rho_G >> \rho$$

$$W - B \doteq W$$

$$m\frac{dv}{dt} \doteq W - f$$

$$\frac{4}{3}\pi a^3 \rho_G \frac{dv}{dt} \doteq \frac{4}{3}\pi a^3 \rho_G g - 6\pi\eta a v$$

$$\frac{dv}{dt} \doteq g - \frac{9}{2}\frac{\pi\eta a v}{\pi a^3 \rho_G}$$

$$\frac{dv}{dt} \doteq g - \frac{9}{2}\frac{\eta}{a^2\rho_G} v$$

$$K = \frac{9}{2}\frac{\eta}{a^2\rho_G}$$

$$\frac{dv}{dt} \doteq g - Kv \qquad \text{(c-1)}$$

The solution to the differential equation (c-1) is

$$v_t = e^{-\int_{t_o}^{t} K d\tau} \int_{t_o}^{t} g\, e^{\int_{t_o}^{t} K d\tau} d\tau + v_o,$$

where t has been replaced by τ as the variable of integration. Take, as boundary conditions,

$$t_o = 0, \quad v_o = 0.$$

Application of the boundary conditions leads to

$$v_t = e^{-\int_{0}^{t} K d\tau} \int_{0}^{t} g\, e^{\int_{0}^{t} K d\tau} d\tau$$

which integrates to give

$$v_t = g e^{-Kt} \left(\frac{1}{K} e^{Kt} \Big|_0^t \right.$$

or

$$v_t = g e^{-Kt} \frac{1}{K} \left(e^{Kt} - 1 \right) .$$

The final solution to equation (c-1) is

$$v_t = \frac{g}{K} \left(1 - e^{-Kt} \right) . \qquad \text{(c-2)}$$

The terminal velocity, v_T , may be obtained from equation (c-2) by making suitable approximations. If $Kt >> 1$, then

$$v_t \doteq \frac{g}{K} = v_T$$

Next,

$$\frac{4}{3}\pi a^3 \rho_6 = m , \qquad a = \left(\frac{3m}{4\pi\rho_6} \right)^{\frac{1}{3}}$$

$$K = \frac{g}{2} \frac{\eta}{\rho_6} \left(\frac{4\pi\rho_6}{3m} \right)^{\frac{2}{3}}$$

$$K = \frac{g}{2} \frac{\eta}{\rho_6^{1/3}} \left(\frac{4\pi}{3} \right)^{\frac{2}{3}} \frac{1}{m^{2/3}} .$$

The expression for K becomes, upon substituting in the numerical values for η and ρ_6 ,

$$K = 1.62 \times 10^{-3} \frac{1}{m^{2/3}} .$$

The velocity of the bead would be given by

$$v_t' = gt$$

if the viscous force were zero and the bead were dropped from rest at the time $t = 0$. The ratio of v_t to v_t' is

$$\frac{v_t}{v_t'} = \frac{g}{gKt} \left(1 - e^{-Kt} \right) = \frac{1}{Kt} \left(1 - e^{-Kt} \right)$$

or

$$Kt \frac{v_t}{v_t'} = \left(1 - e^{-Kt} \right) \qquad \text{(c-3)}$$

which is implicit in t .

The specification of a minimum allowable ratio of v_t to v_t' allows the maximum dropping height for a given mass of bead to be computed if the momentum of the bead is to be known to within a certain percent. Let us choose the maximum allowable ratio of v_t to v_t' as 0.85 so that

$$\frac{v_t}{v_t'} \leq 0.85$$

which corresponds to a maximum allowable error in the momentum of 15%. Equation (c-3) becomes

$$0.85\, k t_c = 1 - e^{-k t_c} \qquad \text{(c-4)}$$

which may be solved for t_c through the use of numerical methods. The value of t_c found by the above procedure may be used to find the corresponding maximum dropping height as given by

$$h_{max} = \frac{1}{2} g t_c^2 .$$

Application of the technique outlined in the preceding paragraphs to calibration beads of various masses leads to the critical values of the parameters of interest. A collection of the critical values of the various parameters used in determining the 15% error curve shown in Figure 22 is arranged in tabular form in Table XVII.

TABLE XVII

NUMERICAL VALUES ASSOCIATED WITH THE NUMERICAL SOLUTION OF EQUATION (c-4)

Mass of Bead (μgm)	Diameter of Bead (μ)	k (sec^{-1})	Time of Descent (sec)	Maximum Height (cm)	Terminal Velocity (cm sec^{-1})
1000	954	0.162	2.1	2.2×10^3	6.1×10^3
500	758	0.257	1.3	8.3×10^2	3.8×10^3
100	443	0.75	0.45	1×10^2	1.3×10^3
50	352	1.19	0.3	4.4×10^1	8.2×10^2
10	205	3.50	0.1	4.9×10^0	2.8×10^2
5	163	5.65	0.06	1.8×10^0	1.7×10^2
1	95	16.2	0.02	2×10^{-1}	6.1×10^1

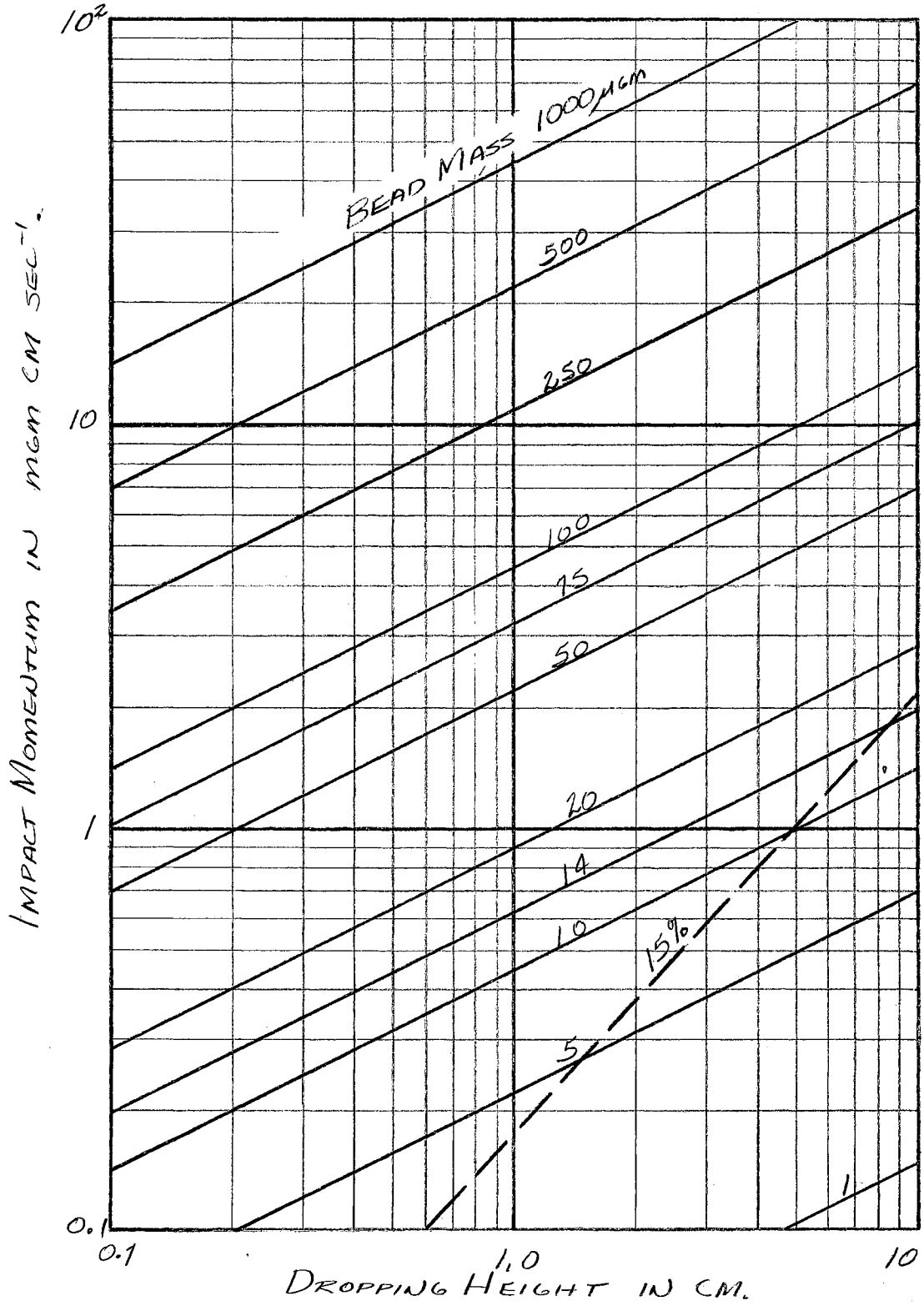

Figure 22. Calibration Aid.

Figure 22 constitutes a convenient aid that may be used during the calibration of a micrometeor detection system. The figure is just a plot of impact-momentum as a function of the dropping height for a given mass of calibration bead. The various solid lines running diagonally across the plot are for different masses of calibration beads, where the beads are dropped in a vacuum. The impact-momentum of a bead dropped in air will be lower than the impact-momentum of the same bead dropped from the same height in vacuum because of the action of the viscous force on the falling bead.

The dropping height for a given mass of bead should be chosen such that both the dropping height and the bead mass do not simultaneously fall below the 15% error curve (the dashed line running diagonally across Figure 22). That is, if the impulse delivered to a rocket skin by a calibration bead is to be known to within 15% accuracy, operation must be above the 15% error curve. The value of 15% was chosen because it corresponds also to the amount of allowable error used as a criterion in determining the minimum altitude at which the micrometeor counts could be considered to be reliable. (See Appendix D).

If the coefficient of restitution for the beads incident on the rocket surfaces is taken to be 0.8, then the impulse delivered to the rocket skin by a calibration bead incident normally on the rocket skin is equal to 1.8 times the impact-momentum as shown in Figure 22 for a given mass of bead and a given dropping height.

APPENDIX D

DECELERATION OF MICROMETEORS BY THE ATMOSPHERE

Collisions between an incoming micrometeor and the air molecules of the atmosphere cause the micrometeor to be decelerated upon entering the atmosphere of Earth. An expression for the deceleration, in which the acceleration due to gravity is neglected, has been developed by Grimminger (11). The expression for the acceleration of the micrometeor is

$$\frac{dv}{dt} = -\Gamma \frac{A}{2m} \rho v^2 \qquad \text{(d-1)}$$

where: Γ is the drag coefficient,

A is the cross-sectional area of the micrometeor,

ρ is the density of the air,

m is the mass of the micrometeor, and

v is the geocentric velocity of the micrometeor.

A change of variables and the introduction of the scale height, H, transforms equation (d-1) into

$$\frac{dv}{v} = -\frac{\Gamma A}{2m} \rho \, dH \qquad \text{(d-2)}$$

where

$$H = \frac{RT}{\mu g} \qquad \text{(d-3)}$$

In equation (d-3), R is the universal gas constant,

T is the temperature on the Kelvin scale,

μ is the molecular weight of the air, and

g is the acceleration due to gravity at height h.

The differential equation (d-2) may be integrated to give

$$\ln v = -\frac{\Gamma A}{2m}\rho H$$

or

$$v = v_6 \exp\left(-\frac{\Gamma A}{2m}\rho H\right) \qquad \text{(d-4)}$$

in which v_6 represents the geocentric velocity of the micrometeor before it enters the atmosphere of Earth.

Now,

$$A = \pi a^2$$

where a is the radius of the micrometeor, and

$$m = \frac{4}{3}\pi a^3 \rho_m$$

where ρ_m is the density of the micrometeor.

Thus,

$$-\frac{\Gamma A}{2m} = -\frac{\Gamma \pi a^2 3}{2(4)\pi a^3 \rho_m} = -\frac{3}{2(4)}\frac{\Gamma}{a\rho_m}.$$

The radius of the micrometeor is given by

$$a = \left(\frac{3m}{4\pi\rho_m}\right)^{1/3}$$

so that

$$-\frac{\Gamma A}{2m} = -\frac{3}{2(4)}\frac{\Gamma}{\rho_m}\left(\frac{4\pi\rho_m}{3m}\right)^{1/3}$$

$$-\frac{\Gamma A}{2m} = -\frac{\Gamma}{2}\left(\frac{9\pi}{16\rho_m^2}\right)^{1/3}\frac{1}{m^{1/3}}.$$

The average density of particles of micrometeoric size is probably about

$$\rho_m \doteq 3.6 \text{ gm cm}^{-3},$$

giving

$$-\frac{\Gamma A}{2m} = -\frac{\Gamma}{2}\left(\frac{9\pi}{16(3.6)^2}\right)^{1/3}\frac{1}{m^{1/3}}$$

$$-\frac{\Gamma A}{2m} = -\frac{\Gamma}{2}(0.515)\frac{1}{m^{1/3}}.$$

The velocity equation, (d-3), has reduced to

$$v = v_6 \exp\left(-\frac{\Gamma}{2}(0.515)\frac{1}{m^{1/3}}\rho H\right) \qquad \text{(d-5)}$$

According to Grimminger (11),

$$\Gamma = \begin{cases} 2 & \text{FOR } h \geq 100 \text{ Km.} \\ 1 & \text{FOR } h < 100 \text{ Km.} \end{cases}$$

Substitution of the numerical values for Γ into (d-5) leads to the two equations:

$$v = v_0 \exp\left(\frac{-0.515}{m^{1/3}} \rho H\right), \quad h \geq 100\ \text{Km} \qquad \text{(d-6)}$$

$$v = v_0 \exp\left(\frac{-0.258}{m^{1/3}} \rho H\right), \quad h < 100\ \text{Km} \qquad \text{(d-7)}$$

both of which are of the form

$$v = v_0 \exp\left(-f(m) \rho H\right).$$

If we take

$$m = 1.25 \times 10^{-10}\ \text{gm},$$

the two equations become

$$v = v_0 \exp\left(-1.03 \times 10^{3} \rho H\right), \quad h \geq 100\ \text{Km}$$

$$v = v_0 \exp\left(-5.2 \times 10^{2} \rho H\right), \quad h < 100\ \text{Km}.$$

Similarly, if

$$m = 1.25 \times 10^{-8}\ \text{gm},$$

the two corresponding equations are

$$v = v_0 \exp\left(-2.22 \times 10^{2} \rho H\right), \quad h \geq 100\ \text{Km}$$

$$v = v_0 \exp\left(-1.11 \times 10^{2} \rho H\right), \quad h < 100\ \text{Km}.$$

Reference should now be made to the tabulation of quantities shown in Table XVIII. These quantities have been abstracted from or derived from the atmospheric data presented by Rocket Panel (12) and Horowitz and LaGow (13). Substitution of some of the data appearing in Table XVIII into the deceleration equations leads to the data tabulated in Table XIX.

TABLE XVIII

ATMOSPHERIC PARAMETERS FOR USE IN DETERMINING
THE DECELERATION OF MICROMETEORS

Γ	Height h (Km)	Data from Rocket Panel (12)				Data from Horowitz and LaGow (13)		
		H (KM)	$\log_{10}\rho$	ρ (GM CM^{-3})	ρH (GM CM^{-2})	H (KM)	ρ (GM CM^{-3})	ρH (GM CM^{-2})
2	160	17.24	-11.781	1.66×10^{-12}	2.86×10^{-6}	37	4.3×10^{-13}	1.59×10^{-6}
	150	15.44	-11.468	3.40×10^{-12}	5.25×10^{-6}	32	6.6×10^{-13}	2.11×10^{-6}
	140	13.68	-11.119	7.60×10^{-12}	1.04×10^{-5}	25	1.2×10^{-12}	3.0×10^{-6}
	130	11.90	-10.720	1.91×10^{-11}	2.27×10^{-5}	15	3.3×10^{-12}	4.95×10^{-6}
	120	10.04	-10.720	5.64×10^{-11}	5.65×10^{-5}	9.4	1.2×10^{-11}	1.13×10^{-5}
	110	8.19	- 9.684	2.07×10^{-10}	1.69×10^{-4}	7.4	5.0×10^{-11}	3.7×10^{-5}
	100	7.26	- 9.065	8.61×10^{-10}	6.25×10^{-4}	6.4	2.5×10^{-11}	1.6×10^{-4}
1	100	7.26	- 9.065	8.61×10^{-10}	6.25×10^{-4}			
	95	6.87	- 8.734	1.85×10^{-9}	1.27×10^{-3}			
	90	6.54	- 8.389	4.08×10^{-9}	2.67×10^{-3}			
	85	6.29	- 8.034	9.25×10^{-9}	5.81×10^{-3}			
	80	6.16	- 7.676	2.11×10^{-8}	1.3×10^{-2}			
	75	6.27	- 7.335	4.62×10^{-8}	2.89×10^{-2}			
	70	6.53	- 7.012	9.68×10^{-8}	6.33×10^{-2}			

TABLE XIX

METEOR VELOCITIES AT VARIOUS ALTITUDES

Mass of Micrometeor (gm)	Alt. h (Km)	Rocket Panel		Horowitz and LaGow	
		ρH (GM CM^{-2})	$\frac{U}{U_0}$	ρH (GM CM^{-2})	$\frac{U}{U_0}$
1.25×10^{-10}	150	5.25×10^{-6}	0.995		
	140	1.04×10^{-5}	0.989		
	130	2.27×10^{-5}	0.977	4.95×10^{-6}	0.995
	120	5.65×10^{-5}	0.944	1.13×10^{-5}	0.988
	110	1.69×10^{-4}	0.840	3.7×10^{-5}	0.963
	100	6.25×10^{-4}	0.525	1.6×10^{-4}	0.848
	100	6.25×10^{-4}	0.725		
	95	1.27×10^{-3}	0.520		
	90	2.67×10^{-3}	0.252		
	85	5.81×10^{-3}	0.050		
	80	1.3×10^{-2}	0.0012		
	75	2.89×10^{-2}	10^{-5}		
1.25×10^{-8}	120	5.65×10^{-5}	0.987	1.13×10^{-5}	0.997
	110	1.69×10^{-4}	0.963	3.7×10^{-5}	0.992
	100	6.25×10^{-4}	0.870	1.6×10^{-4}	0.965
	100	6.25×10^{-4}	0.933		
	95	1.27×10^{-3}	0.868		
	90	2.67×10^{-3}	0.744		
	85	5.81×10^{-3}	0.525		
	80	1.3×10^{-2}	0.237		
	75	2.89×10^{-2}	0.040		
	70	6.33×10^{-2}	0.0009		

VITA

Curtis W. McCracken

Candidate for the Degree of

Master of Science

Thesis: AN ANALYSIS OF ROCKET AND EARTH SATELLITE MEASUREMENTS OF MICROMETEORIC INFLUX

Major Field: Physics

Biographical:

Personal Data: Born near Vici, Oklahoma, on 7 June 1934, the son of Eugene C. and Arta V. McCracken.

Education: Attended grade school and high school at Vici, Oklahoma; graduated from Vici High School in May, 1952; received the Bachelor of Science Degree in Mathematics from Panhandle Agricultural and Mechanical College, Goodwell, Oklahoma, in May, 1956; completed the requirements for the Master of Science Degree in Physics from Oklahoma State University, Stillwater, Oklahoma, in May, 1959.

Organizations: Member of Lambda Sigma Tau, Kappa Kappa Psi, Sigma Pi Sigma, and Who's Who in American Colleges and Universities.